Master's thesis

NTNU
Norwegian University of Science and Technology
Faculty of Information Technology and Electrical Engineering
Department of Electric Power Engineering

Martine Johanne Nordengen Baksvær

EMD and Online EMD for Harmonic Detection in Power Systems

Master's thesis in Electric Power Engineering
Supervisor: Olav Bjarte Fosso
Co-supervisor: Paula Bastos Garcia Rosa
June 2019

NTNU
Norwegian University of Science and Technology

Martine Johanne Nordengen Baksvær

EMD and Online EMD for Harmonic Detection in Power Systems

Master's thesis in Electric Power Engineering
Supervisor: Olav Bjarte Fosso
Co-supervisor: Paula Bastos Garcia Rosa
June 2019

Norwegian University of Science and Technology
Faculty of Information Technology and Electrical Engineering
Department of Electric Power Engineering

Preface

This master thesis was completed in the spring 2019 at the Department of Electric Power Engineering and concludes the authors studies at the Norwegian University of Science and Technology.

I, the author, would like to express my deepest appreciation to all those who have who have provided me the possibility to complete this thesis. A special gratitude to my supervisor Professor Olav Bjarte Fosso for introducing me to the world of signal analysis and the possibilities this world provides. He has inspired and motivated me through the process and has been extremely supportive. Through encouraging meetings he has built my confidence and sheared of his experience and knowledge. I would also like to thank my co-supervisor Postdoctoral Researcher Dr. Paula Bastos Garcia Rosa, for the great support. She has provided necessary help in MATLAB and she has sheared of her experience with Online EMD which has been of great value for my work.

I would also like to thank my father Arnfinn for bringing me along to his work at hydro power plants as a kid and hence sparking my interest in electric power. If it was not for him, I might have chosen a different career path, which would not have been as electrifying.

Trondheim, June 2019

Martine Johanne N. Baksvær

Abstract

In this thesis, power system harmonics and detection methods for power system harmonics have been investigated. Harmonics have been an issue in power systems for a very long time, but due to the increasing use of nonlinear loads, like power electronic converters, the harmonic pollution have increased. Electrical grids where new type of components interact are becoming prone to harmonic pollution as well. Harmonics can cause severe damage to components in the power system, like overheating of components or false tripping of circuit breakers, and thus, it should be reduced. A mathematical model that describes accurately the physical behaviour of harmonics can be a challenging task in a large scale system. Even if a detailed mathematical model is available, such model can be of high order and can result in a complex controller. As an alternative to high fidelity modelling, this thesis is based on data analysis and on-line identification techniques that can characterize the grid under operation.

There are several methods available for harmonic detection, and in this thesis, the empirical mode decomposition (EMD) is investigated. This method, unlike the commonly used fast Fourier transform (FFT) method, is a more recent developed method that was designed to handle both non-linearity and non-stationarity. In addition to the standard EMD, an online version of the method is investigated. This extension of the EMD is a method that enables analysis of data streams, which may be suitable for on-line harmonic detection and control purposes.

Standard EMD decomposes a signal into a number of intrinsic mode functions (IMFs), which are different modes of oscillation. After the decomposition is complete, the frequencies of each IMF can be calculated and the harmonic components of the signal can be detected. In the online extension of the EMD, the extraction of modes is done blockwise through a sliding window that enables analysis of data flows in real-time with some delay.

In this thesis, EMD has been applied to a current measurement using both a Python code and MATLAB code, which revealed differences in the decomposition. The Python code was able to identify all the frequency components of the current measurement, while the results obtained with MATLAB suffered from mode mixing. A duplication of the current measurement was made in order to make it suitable for the online EMD. This duplication was analyzed using the standard EMD, both in Python and MATLAB, and online EMD. When the measurement was duplicated, mode mixing became an issue for both codes. In order to investigate why mode mixing occurred, a synthetic signal mimicking the current measurement was constructed and analyzed with the online EMD. It was found that if the amplitudes of the harmonic components were doubled, the mode mixing disappeared. For real-time applications, it is important to know the time lag of the online EMD decomposition. Thus, the time lag for a synthetic signal without mode mixing is examined.

Sammendrag

I denne avhandlingen har harmoniske komponenter og deteksjonsmetoder for harmoniske komponenter i kraftsystemer blitt undersøkt. Harmoniske komponenter i kraftsystem har vært et problem i lang tid, men på grunn av den økende bruken av ikke-lineære laster, som kraftelektroniske omformere, har mengden av harmoniske komponenter økt. I tillegg blir kraftnett hvor nye typer komponenter interagerer også utsatt for forplantning av harmoniske komponenter. Harmoniske komponenter kan forårsake alvorige skader på komponentene i kraftnettet, som for eksempel kan det forårskaje overoppheting av komponenter eller feilaktig utkobling av strøm brytere, og de bør dermed reduseres. En matematisk modell som beskriver de harmoniske komponentenes oppførsel nøyaktig kan være kompleks og utfordrende å beskrive. Selv om en slik matematisk modell eksisterer kan en slik modell være av høy orden og kan resultere i en kompleks kontroller. Som et alternativ til slik modellering vil denne oppgaven benytte seg av data analyse og on-line identifikasjonsteknikker som karakterisere kraftnetet under drift.

Det er flere tilgjengelige metoder for å detektere harmoniske komponenter, og i denne avhandlingen vil *empirical mode decomposition* (EMD) bli undersøkt. Denne metoden, i motsetning til den hyppige brukte metoden *fast Fourier transform* (FFT), er en nyere utiklet metode som ble designet for å håndtere både ikke-linearitet og ikke-stasjonæritet. I tillegg til standard EMD vil en on-line versjon av metoden bli undersølt. Denne versjonen av EMD er en metode som muliggjør analyse av datastrømmer, som kan være egnet for å detektere harmoniske komponenter i sanntid og kontrollformål.

Standard EMD dekomponerer et signal til en rekke modusfunksjoner kalt *intrinsic mode functions* (IMFs), som er forskjellige svingemoduser. Etter at dekomponeringen er fullført, kan frekvensene for hver IMF beregnes og signalets harmoniske komponenter kan detekteres. For online EMD detekterer moduser blokkvis gjennom et glidende vindu som muliggjør analyse av datastrømmer i sanntid, dog med en tidsforsinkelse.

I denne oppgaven har EMD blitt anvendt på et målt strømsignal ved hjelp av både en Python-kode og MATLAB-kode, hvor forskjeller i dekomponeringen ble funnet. Pythonkoden var i stand til å identifisere alle frekvenskomponentene til strømsignalet, mens resultatene som ble oppnådd med MATLAB led av blanding av modusene (mode-mixing). En forlenging av strømsignalet ble gjort for å gjøre den egnet for online EMD. Denne forlengingen ble analysert ved hjelp av standard EMD, både i Python og MATLAB, og online EMD. Når signalet ble forlenget, ble mode-mixing et problem for begge kodene. For å undersøke hvorfor mode-mixing oppstod, ble et syntetisk signal som imiterer strømsignalet konstruert og analysert med online EMD. Det ble funnet at hvis amplitudene til de harmoniske komponentene ble fordoblet, var det ingen mode-mixing. For sanntidsapplikasjoner er det viktig å vite tidsforsinkelsen av online EMD fører med seg. Derfor ble tidsforsinkelsen for et syntetisk signal uten mode-mixing undersøkt.

Contents

List of Tables

List of Figures

Chapter 1

Introduction

1.1 Motivation

Power systems operates at a fundamental frequency of 50 Hz or 60 Hz, depending on the location of power system. Ideally, the current and voltage waveforms would be pure sinusoidal. However, integer multiples of the fundamental frequency may also be present, making the sinusoid distorted. These integer multiples of the fundamental frequencies are a form of electrical pollution, and are known as power system harmonics [1]. Power system harmonics originate due to various operations, for example, ferroresonance, magnetic saturation, synchronous resonance, and nonlinear and electrically switched loads [2]. Power systems harmonics have been an issue for many years, but in recent years the pollution has increased due to the increased use of nonlinear loads. In addition, electrical grids (e.g., microgrids, marine vessels, offshore platforms, solar farms, wind farms) where several new type of components (power electronic converters, passive components) interact, are becoming prone to harmonic pollution as well. The harmonics can have severe impact on different components in the power system, and they should therefore be properly detected, and procedures should be made to reduce the propagation. A mathematical model that describes accurately the physical behaviour of harmonics in power systems can be a challenging task in a large scale system. Even if a detailed mathematical model is available, such model can be of high order.

As an alternative to high fidelity modelling, there are several different data analysis methods available for detecting power system harmonics, and one of the most commonly used method is the fast Fourier transform (FFT). Even though this methods has provided prominent results, the FFT is limited to linear and stationary signals. A method that handles both nonlinear and non stationary signals is the empirical mode decomposition (EMD) [3]. Due to its adaptive decomposition nature, it has been applied to a variety of research areas e.g, for medical and seismic signal analyses [4]. A number of extensions of the EMD method

are currently available, like local EMD, ensemble EMD and sliding EMD. An extension of the EMD method that can be applied to data streams, and hence may be suitable for direct control purposes, is the online EMD [5]. This method applies EMD to a window of the data, then the window is shifted.

In order to reduce the harmonic propagation in power systems there are several solutions, and in [6] two types of solutions are described. The first solution that is mentioned is to reduce the propagation of harmonics by designing the nonlinear devices for low levels of harmonic distortion. The second solution that is mentioned is to install harmonic compensation equipment at the terminals by the use of filters. There are several types of filters that can be used for such compensation, and a choice must be made based on factors like the power and voltage ratings. One type of filter that can be used for harmonic compensation is the shunt active filter [7]. This is a filter that can be connected as shown in Figure 1.1. In order for the shunt active filter to work properly, a reference current must be computed, and in [8] a version of an online EMD method is used to compute the reference current.

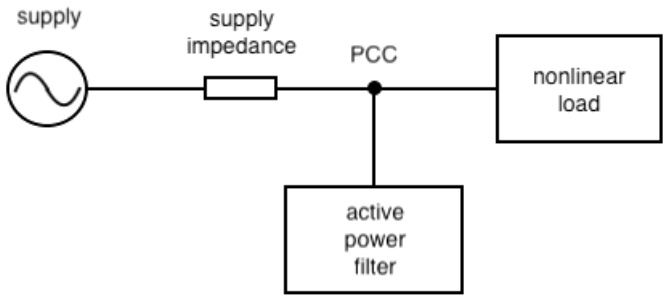

Figure 1.1: Shunt APF. APF connected at point of common coupling (PCC) [7].

The version of the online EMD used in [8] is not the same version of the online EMD that will be investigated in this thesis, but the research performed in this reference is a motivating factor for wanting to investigate the online EMD presented in [5].

1.2 Objectives

The aim of this work is to evaluate the decomposition provided by the EMD, and one of its extensions - the online EMD, for a real signal containing harmonics. The online EMD allows the analysis of data streams, which can be beneficial for real-time harmonic detection and control purposes. However, the decomposition of the online EMD has a time delay that should be estimated if the aim is to use the resultant signals for control purposes. Thus, this work also aims to investigate the time delay of the online EMD decomposition of a signal containing harmonics.

1.3 Limitations

The current measurement that is analyzed is a short measurement of only 0.05 seconds. In order to make it suitable for the Online EMD the current measurement is duplicated a number of times. The thesis is limited to analysis of this particular measurement, the duplication and synthetic versions of it. The programming will be performed in both Python and MATLAB.

The theory presented in this thesis is what the author means is necessary for the reader to know before continuing on to the analysis and results. For a reader with little experience in signal analysis in power systems, the author recommends to review the references presented in each section for a more detailed description if necessary.

1.4 Structure of thesis

- Chapter 2: in this chapter, theory about the concept of harmonics, the problems they can cause and harmonic interaction is presented.
- Chapter 3: in this chapter, an introduction to methods used for analysis in electrical power systems is giver. In addition to this, some of the most common methods for harmonic detection is presented.
- Chapter 4: in this chapter, the standard EMD method is presented. It includes some drawbacks and some extensions of the method.
- Chapter 5: in this chapter, the Online EMD method is presented with its algorithm and information about the execution time.
- Chapter 6: in this chapter, the Hilbert transform and an algorithm for calculation of the instantaneous frequency is presented.
- Chapter 7: in this chapter, an analysis using the standard EMD and the Online EMD is presented. Both the methods are applied to current signals containing harmonics, and the results are discussed.
- Chapter 8: in this chapter, the conclusion of the analysis is presented, and some remarks on further work is given.

Chapter 2

Harmonics

With increasing use of power electronic equipment in modern industry to achieve higher reliability and efficiency in power systems, there is also an increasing propagation of harmonics. Even though harmonics are becoming an increasing issue, it is not a new concept. The first ones to ever use the word *harmonic* was Houston and Kennelly in 1894 [9]. They did not use any equations to describe the concept, but presented the properties of of periodic curves. Problems caused by harmonic components of voltage and current have been an issue for power engineers for over 100 years:

> *"We operating men, I think, all agree that we have harmonics. I think we all agree that, like the poor, the harmonics will always be with us. If we could get rid of them, we would be very glad to do so. "*
>
> *- J.B Fisken (Sept. 8, 1916) [10]*

The concept of harmonics and harmonic interaction have been presented in [11], but they will included here as well.

2.1 Concept of harmonics

Harmonics are a major concern in power systems, as harmonics cause distortion in voltage and current waveforms [12]. Harmonics refer to components of a waveform that are integer multiples of the fundamental frequency [13]. As a result of this, the frequency of a harmonic, f_h, can be found as:

$$f_h = h \cdot f_n \tag{2.1}$$

where h is an integer and f_n is the fundamental frequency. If the fundamental frequency is, for example, 50 Hz, the 6^{th} would have a frequency of:

$$f_6 = 6 \cdot 50Hz = 300Hz$$

In addition to integer multiple of the fundamental frequency, which is known as harmonics, there is also a phenomenon called interharmonics which are non-integer multiples of the fundamental frequency. A main source of interharmonics are AC/AC converters [12].

Harmonics are caused by loads that draw non-sinusoidal current from a sinusoidal voltage source. Examples of loads that produce harmonics are static VAR compensators, inverters, converters, electric arc furnaces and AC or DC motor drives. [13]

2.2 Fourier Series

A periodic function, $f(t)$, can be expressed as $f(t) = f(t+T)$ [12]. This function can be represented by a series of elements that consists of a DC component, other frequencies that include the fundamental frequency component and its harmonics. This applies if the Dirichlet conditions are met:

1. $f(t)$ has a finite mean value over a period, *T*.
2. $f(t)$ has a finite number of positive and negative maximum values.
3. $f(t)$ has a finite number of discontinues over a period, *T*.

The trigonometric series, $f(t)$, can be expressed as:

$$f(t) = \frac{a_0}{2} + \sum_{h=1}^{\infty}[a_h cos(h\omega_0 t) + b_h sin(h\omega_0 t)] \tag{2.2}$$

where $\omega_0 = 2\pi/T$.

The expression in equation (2.2) can be simplified to:

$$f(t) = c_0 + \sum_{h=1}^{\infty} c_h sin(h\omega_0 t + \phi_h) \tag{2.3}$$

where

$$c_0 = \frac{a_0}{2}, c_h = \sqrt{a_h^2 + b_h^2}, \quad \text{and} \quad \phi_h = tan^{-1}(\frac{a_h}{b_h})$$

$h\omega_0$ is the h^{th} order harmonic of the periodic function, c_0 is the magnitude of the DC component, c_h is the magnitude of the h^{th} harmonic component and ϕ_h is the phase of the h^{th} harmonic component.

Equation (2.3) is the Fourier series and it describes the periodic function that consists of the contribution of sinusoidal functions with different frequencies and amplitudes.

2.3 Problems caused by harmonics

There are several problems caused by both harmonic currents and voltages. They can cause problems both in the power system and in the installation itself. The problems are wide in range and some of them will be presented here.

2.3.1 Problems caused by harmonic currents

Neutral conductor over-heating can be an issue if the *triple-N* harmonic currents are present in a three-phase system. These will add in the neutral which can cause overheating [14]. Figure 2.1 illustrates such harmonics.

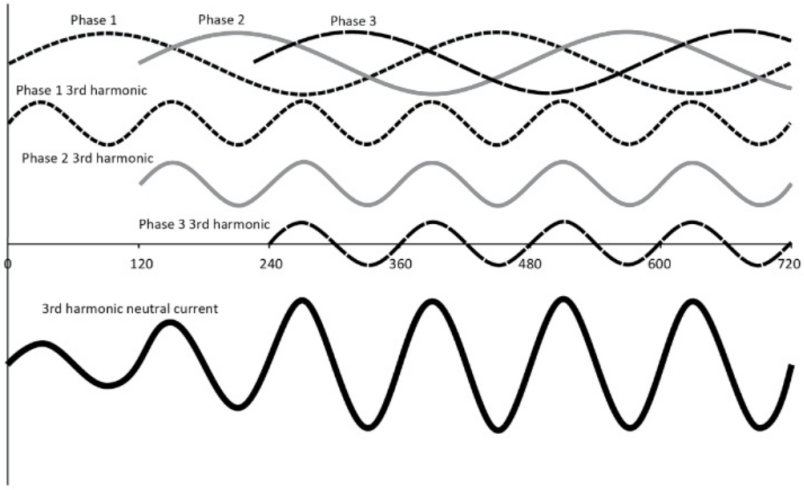

Figure 2.1: Triple-N Harmonic currents in the neutral [14].

Nuisance tripping of circuit breakers can occur in residual current circuit breakers (RCCB) due to the presence of harmonics for two reasons. Firstly, the RCCB is an elecromecanical device and may not sum higher frequency components correctly, and hence, trip. Secondly, equipment that generate harmonics may also generate switching noise that must be filtered at the power connection of the equipment [14].

Skin effect is when an alternating current flows on the outer surface of a conductor. For power supply frequencies, skin effect is usually not a problem, but for frequencies above 350 Hz, i.e the seventh harmonic, skin effect may occur. Skin effect causes losses and heating, and should be avoided [14].

Overheating of transformers can be caused by the presence of harmonics. When harmonics are present in a transformer, eddy current losses increases. In fact, the eddy current losses will increase with the square of the harmonic number. Increased eddy current losses will lead to a higher operating temperature and a shorter life time for the transformer [14].

2.3.2 Problems caused by harmonic voltages

Voltage distortion of the supply voltage can occur when a non-linear load draws a distorted current which causes a non-sinusoidal voltage drop in a circuit impedance. The distorted voltage causes distorted current flow in linear loads which can affect performance or efficiency. Figure 2.2 illustrates this behaviour, where the voltage distortion is assumed to be zero at the point of common coupling(PCC). This is not the case in real applications as the supply network has impedance and carries distorted currents and hence the supply voltage is always distorted.[14]

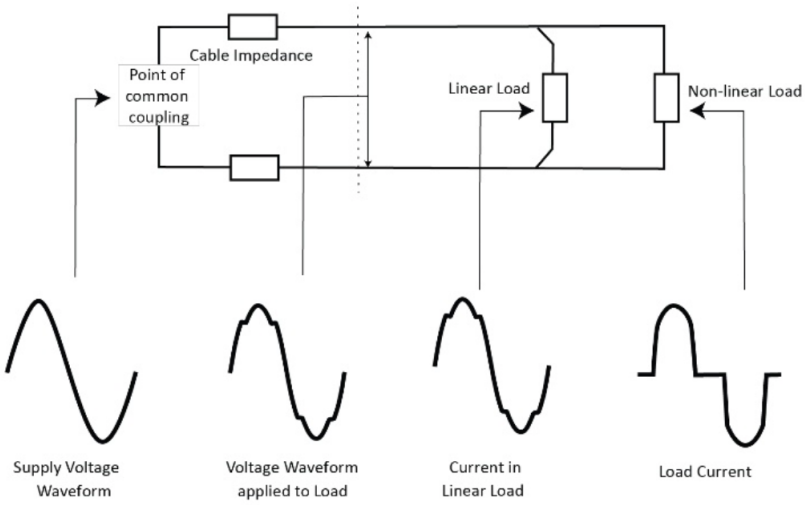

Figure 2.2: Voltage distortion caused by a non-linear load [14]

Zero-crossing noise can be an issue for electronic controllers that determine when loads should be turned on by detecting the zero-crossing of the supply voltage. If transients or harmonics are present, it is more difficult to detect the zero-crossing of the supply voltage as there may be several zero-crossings per cycle caused by the distorted voltage [14].

2.4 Harmonic interaction

In addition to the harmonics caused by non-linear loads, there is a concern that harmonics may interact between large numbers of power inverters and the distribution network. Studies [15] have shown that this is in fact an issue especially for large populations of PV inverters, which can cause problems for microgrids where PV is a common resource. Under certain circumstances with presence of high penetration of PV inverters, the PV inverters have switched of undesirably or the harmonic emissions have increased significantly. As a result of this, the power quality standards set for the PCC are exceeded even though all the inverters individually satisfy their specifications. For networks with a large number of PV inverters, the resonance phenomenon can be characterised by parallel resonance and series resonance.

Parallel resonance of the supply inductance L_p, parallel network capacitance C_p, resulting from distortion that is generated internally, i.e, as illustrated in Figure 2.3(left). The PV inverter can be assumed to be the source of the harmonic generation. In this case, the impedance at the resonance is high, which results in higher voltage distortion at the PCC, or where the PV inverter is connected to the load [15].

Series resonance of the supply inductance L_p, parallel network capacitance C_p, resulting form distortion that is generated externally or that is injected, as illustrated in Figure 2.3(right). Here, the mechanism is the background supply voltage distortion. In this case the impedance at the resonance is low, which results in higher current distortion through the load and PV inverter capacitor [15].

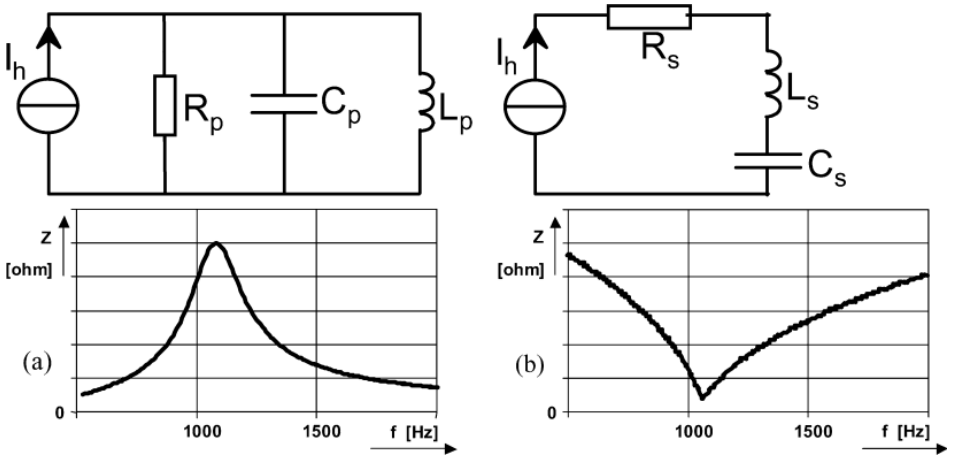

Figure 2.3: Mechanisms of parallel resonance (left) and series resonance (right) [15].

In practice both the resonance phenomenons are linked in one circuit hence causing measuring of both increased voltage and current. The series and parallel resonance can be calculated by:

$$f_r = \frac{1}{2\pi\sqrt{LC}} \tag{2.4}$$

where f_r is the resonance frequency and L and C are respectively the equivalent reactance and capacitance in the parallel or series network.

If the PV inverter generates a harmonic (parallel resonance mechanism), which corresponds to the parallel resonance frequency, then high resonance voltage will occur in the network at the PCC. As a result of this, the operation of the PV inverter and equipment connected to the PCC may be effected. If the power network is weak, i.e, L is large, the resonance may be even more severe resulting in a lower frequency parallel resonance. If the network background distortion contains a harmonic (series resonance mechanism), which corresponds to the series resonance frequency, high resonance current will flow in the network. As an example of the effect, one can assume that if there are 10-30 households with PV installed on the roof tops and that these are all on one phase of a single 400 V cable feed, the natural frequency can be as low as the 5^{th} harmonic (250 Hz) [15].

2.4.1 Inverter topologies

In [16], PV inverters are described as single-phase self-commutated voltage source converters in the 1-5 kW for individual households. These inverters are summarised in Figures 2.4 and 2.5, and the following description:

1) Single-stage pulse-width-modulated (PWM) DC/AC converter topology (H-bridge or Push-Pull) that is directly coupled to the grid through a low frequency (LF) isolation transformer and filter. This can be seen in figure 2.4.

2) Multi-stage topology of PWM DC/AC converter front-end including a high-frequency (HF) isolation transformer, a high frequency rectifier, a line frequency unfolding bridge coupled to the network through small filter components. This can be seen in figure 2.5.

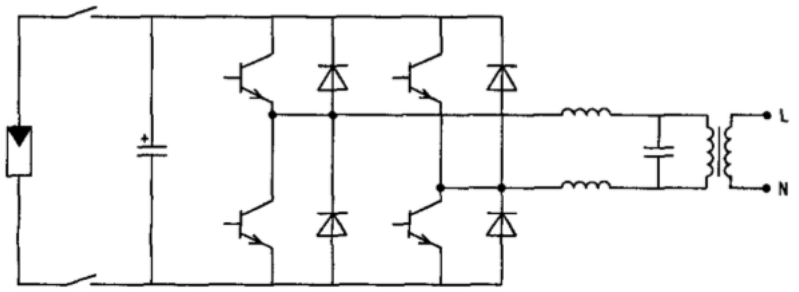

Figure 2.4: Single-stage H-bridge PWM converter and line frequency transformer and filter elements [16].

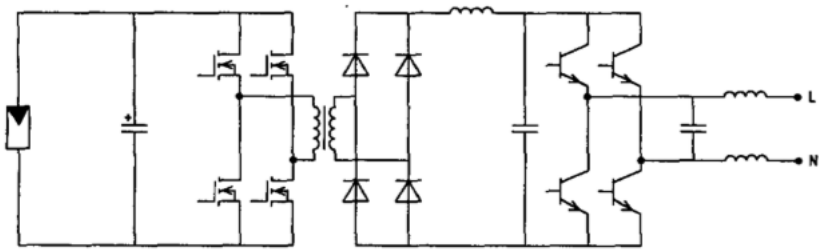

Figure 2.5: Multi-stage converter with high-frequency transformer and low-frequency unfolding bridge [16].

2.4.2 Network simulations

A dutch residential network that includes 197 homes with PV arrays and inverters installed is a basis for a study of possible PV interaction issues is presented in [15]. A part of this network (VP4) was modelled an can be seen in Figure 2.6. This section of the network includes a 10 kV - 400 V transformer and houses with different type of PV inverters. In this model, houses with the same inverter topology were modelled as one single model.

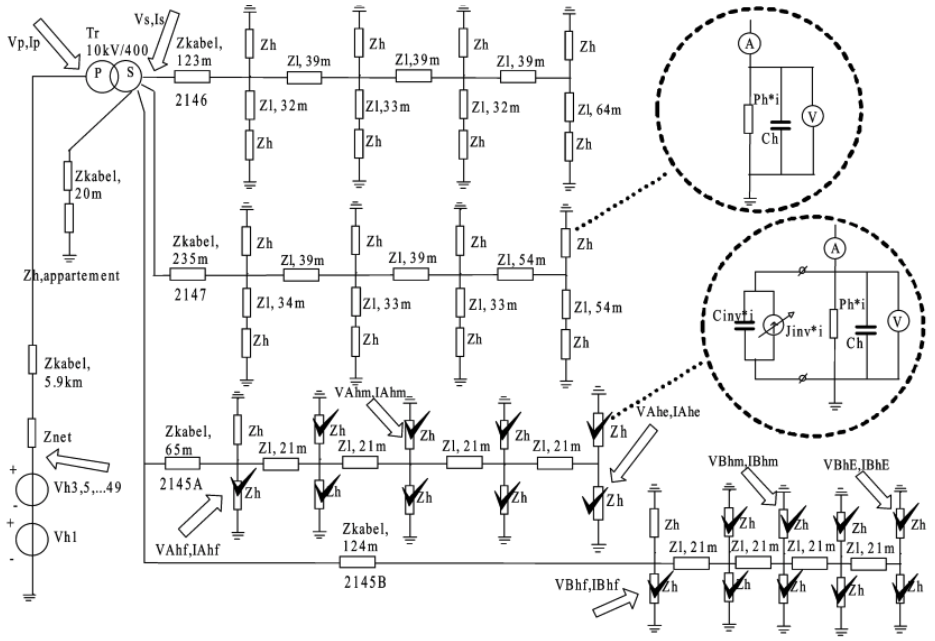

Figure 2.6: Model of network (VP4) with inverters [15], [16].

A simulation with this network , shown in Figure 2.6, was completed with the Dutch national average background distortion (THD = 3%). In order to keep the voltage within the regulation limits, the voltage, V_{main}, was reduced by 2 %. The result of this simulation is shown in Figure 2.7, which shows a clear current distortion and some distortion of the voltage. The network was also tested for maximum allowed distortion, and the result can be seen in Figure 2.8. The results show voltage distortion and severe current distortion.

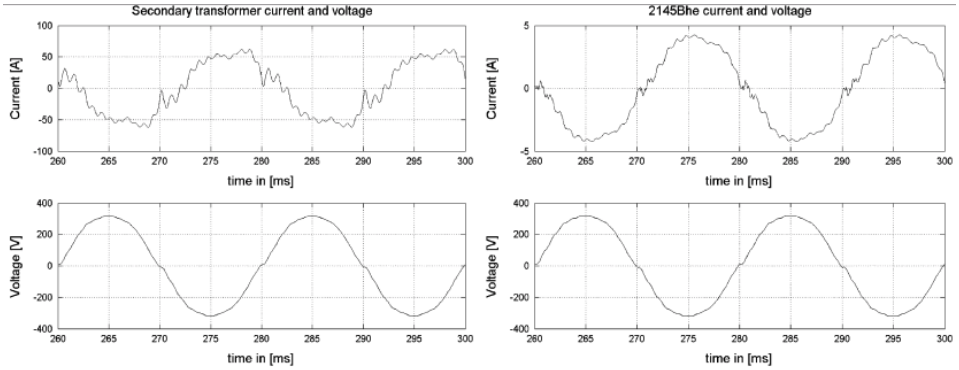

Figure 2.7: Simulation results for two locations in the network section (VP4) with average background distortion ($V_{main} - 2\%$)[15].

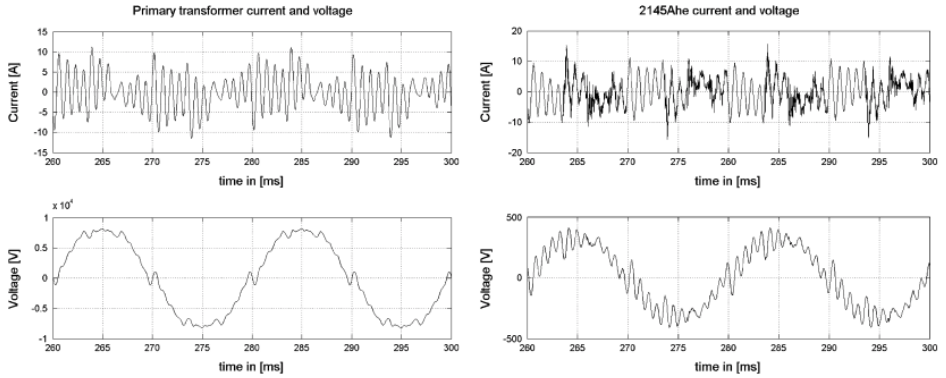

Figure 2.8: Simulation results for two locations in the network section (VP4) with maximum allowable distortion [15].

Chapter 3

Electrical power systems - classification of methods for analysis

There are several methods available for signal analysis in power systems. In Figure 3.1 a tree diagram shows the classification of some of these methods. As seen in this figure, there are two top-level classifications, *Ambient operation* and *Transient operation*, which refers to the system response which they are applicable. In this chapter, an overview of classification of methods for electrical power systems is presented. The classification, and the explanation of the different methods is from [17] where additional information can be found.

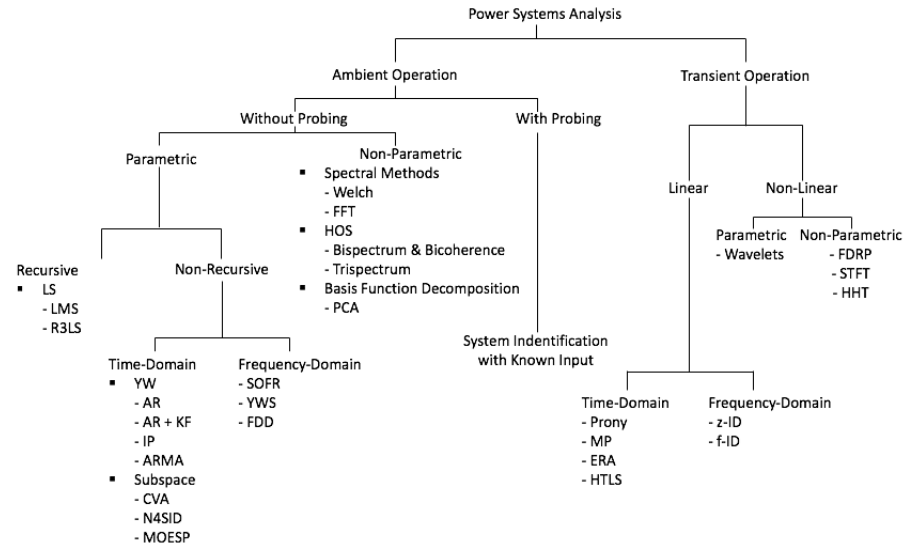

Figure 3.1: Tree diagram showing classification of methods for power system analysis [17]

3.1 Ambient

As mentioned, the classification is divided into two top-levels, *Ambient Operation* and *Transient Operation*. Ambient operation refers to when the system is assumed to be fairly linear and the variation of load approximately random and Gaussian. The variations of load are made by the consumers when they turn their electric equipment ON and OFF. These changes cause a disturbance that is continuous and has small amplitude. When performing measurements during ambient operation, the signals are stochastic in nature and dominated by broadband noise. This originates in the load side, and since the load cannot be measured everywhere in the system, the input is assumed to be unknown. When performing an analysis during ambient operation, the goal is to determine the damping of the system. This is done by using the measurements, which can be difficult to obtain by the outputs only. A solution to this is to apply probing. Therefore, the methods for ambient operation can be divided into methods that require probing and methods that does not require probing, as illustrated in Figure 3.1.

3.1.1 Methods that require probing

Probing is done by injecting an external disturbance into a system through a large load of an interconnector and measuring the response of the system. The probing signal is taken as input and the measurements are taken as the output of the system. The system response is then calculated using basic input-output system theory.

3.1.2 Methods that do not require probing

As illustrated in Figure 3.1, the methods that do not require probing can be further divided into *non-parametric* and *parametric* methods. Parametric methods are methods that aims to fit the signal to a model. In order to obtain this, there must be an assumption on how the signal behaves. Contrarily, non-parametric methods do not fit the signal to a model, and they are only related to the signal. Non-parametric methods can be used to estimate mode frequencies in data, but are not suitable for estimating damping coefficients. By looking at the tree diagram in Figure 3.1 again, it shows that the parametric methods can be further divided into *recursive* and *non-recursive* methods. Recursive methods converge to a solution for the model parameters with respect to time and uses a new set of data to update the previous calculated solution. Non-recursive methods re-calculates a new solution for each new set of data. The non-recursive methods can further be divided into *Time-Domain* and *Frequency-Domain* approaches (Figure 3.1). The time-domain methods use the measurement time series directly whereas the frequency-domain methods use the spectra of the measurements.

3.2 Transient

The other top-level is as mentioned transient operation. Transient operation refers to the power system response after a fault has occurred or a large disturbance has been initiated. During this operation there are large deviations in measurable system parameters, for example, in the frequency. It is assumed that the transient after a fault or a disturbance represents the actual impulse response of the system. Thus, the aim of transient analysis is to measure the stability of the system by determining the oscillatory frequency and the damping of the transient. As illustrated in Figure 3.1, transient methods are sub-divided into *linear* and *non-linear* methods.

3.2.1 Linear methods

Linear methods assume that after a fault or a disturbance, the system is still linear. The purpose of the method is to fit a model of a sum of decaying sinusoids to the transient data. The measured output *y(t)* is made out of a weighted sum of *n* decaying sinusoids λ_i, with weights B_i, where λ_i can be decomposed into a frequency component ω_i and a exponential decay component α_i.

$$y(t) = \sum_{i=1}^{n} B_i e^{\lambda_i t}$$

The linear methods can be divided into *time-domain* and *frequency-domain* methods. The difference between these two classifications is that the time-domain methods fit a linear

model to the data by analyzing the time-series of the data, whereas the frequency-domain methods fit a linear model to the data by analyzing the frequency spectra of the data.

3.2.2 Non-linear methods

In comparison to the linear methods, non-linear methods assume that after a fault or disturbance, the response is mainly non-linear. Non-linearity in this case refers to the interactions between the frequency components in the transient response. Non-linear methods aim to track the change of frequency and damping over a short period of time. As seen in Figure 3.1, the non-linear methods can be sub-divided into parametric methods, which provide specific values for the damping modes, and non-parametric methods, which does not provide this information.

3.3 Harmonic detection methods in power systems

The purpose of harmonic detection methods is to predict the harmonic distortion, at one or more locations, in the power network [9]. Analysis of harmonics is often carried out in order to estimate the effect of a new non-linear load or if a harmonic filter is going to be installed. There are several methods available for harmonic detection, and in this section, the most common methods will be mentioned. Methods for harmonic detection in active power filters (APFs) can be classified relative to the domain where the mathematical model is developed, time-domain and frequency-domain. Some of the most common methods are listed In table 3.1. The time-domain methods, compared to the frequency-domain methods, require fewer calculations and are hence used when speed is an important factor. The frequency-domain methods are traditionally identified with Fourier analysis. Because of the growing pollution of harmonics in power systems and the wish to reduce harmonics, there are several attempts to find more efficient and cost effective solutions for harmonic detection. Some examples of other methods can be seen in [18, 19, 20]

Table 3.1: Classification of typical harmonic detections in APF [21].

Domain	**Harmonic detection method**
Time-domain	- Synchronous fundamental dq-frame - Synchronous individual harmonic dq-frame - Instantaneous power pq-theory and variants - Generalized integrators and variants
Frequency-domain	- Discrete Fourier Transform (DFT) - Fast Fourier Transform (FFT) - Recursive Discrete Fourier Transform (RDFT)

As seen in Table 3.1, the Fourier transform is a typical detection method for harmonics. The Fourier transform, in different versions, is a method that is easy to implement and

is a method that is commonly used for analyzing global energy-frequency distributions. Fourier spectral analysis has dominated i data analysis almost the entire time since it was first introduced, and it has been applied to all sorts of data [3]. Even though the method has shown valid results under a variety of conditions, there are some drawbacks of the Fourier spectral analysis. In order for the Fourier spectrum to make physical sense, the following two requirements must be fulfilled:

1. The system must be linear.
2. The data must be strictly periodic or stationary.

Linear systems. A linear system implies two conditions:

- Homogeneity.
- Superposition.

A state of a system defined in the state equation form can be considered as:

$$\dot{x} = f[x(t), r(t), t] \tag{3.1}$$

If $x(t)$ is the solution to this differential equation with initial conditions $x(t_0)$ when t = t_0 and the input $r(t)$, $t > t_0$:

$$x(t) = \varphi[x(t_0), r(t)] \tag{3.2}$$

then homogeneity implies that

$$\varphi[x(t_0), \alpha r(t)] = \alpha\varphi[x(t_0, r(t))] \tag{3.3}$$

where α is a scalar constant [2].

The superposition implies that the following relation $f(t) + g(t)$ describes a linear system even though $f(t)$ and $g(t)$ are non-linear functions of the variable t [22].

Stationarity. The requirement of stationarity is not only a requirement for the Fourier spectral analysis, but also for many other data analysis methods [3]. A time series $X(t)$

$$X(t) = [x(t_0), X(t_1), ..., X(t_{N-1})] \tag{3.4}$$

is strongly stationary if the joint probability

$$P(x(t)) = P(X(t_N - t_{N-1}, ..., t_1 - t_0)) \tag{3.5}$$

only depend on the time differences $\tau = t_{n+1} - t_n$ for all $n = 0, ..., N - 1$

A time series, *X(t)*, is weakly stationary if, for all t,

$$\left.\begin{aligned} E(|X(t)^2|) &< \infty, \\ E(X(t)) &= m, \\ C(X(t_1), X(t_2)) = C(X(t+\tau), X(t_2+\tau)) &= C(t_1 - t_2), \end{aligned}\right\} \tag{3.6}$$

where, E() is the expected value and C() is the covariance function.

Not many data sets from artificial sources or natural phenomena satisfy these definitions. However, Fourier spectral Analysis is still used to examine such data, which may produce misleading results [3].

There are several methods available for analysis of non-stationary data, and a few of them are listed below. Even though these methods solves the issue of stationarity, some of them depend on Fourier analysis, and are hence limited to linear systems. A review of the methods listed below, and some other methods, can be seen in [3].

- The spectrogram; which is a limited time window-width Fourier spectral analysis that obtains a time-frequency distribution by applying a sliding window along the time axis.
- The wavelet analysis; which is generally defined as:

$$W(a, b; X, \psi) = |a|^{-1/2} \int_{-\infty}^{\infty} X(t)\psi^*(\frac{t-b}{a})dt, \tag{3.7}$$

  where ψ^* is the basic wavelet function, *a* is the dilation factor and *b* is the translation of the origin. The definition in Equation (3.7) is quite complex and might be difficult to understand, so a physical explanation is: *W(a,b;X,ψ)* is the *energy* of *X* of scale *a* at *t* = *b*.
- The Wigner-Ville distribution; which can be defined as the Fourier transform of the central covariance function. The central covariance of any time series, *X(t)*, can be defined as:

$$C_c(\tau, t) = X(t - \frac{1}{2}\tau)X^*. \tag{3.8}$$

  Then the Wigner-Ville distribution can be defined as:

$$V(\omega, t) = \int_{-\infty}^{\infty} C_c(\tau, t)e^{-j\omega\tau}d\tau. \tag{3.9}$$

In addition to the methods listed above and the other methods presented in [3], a method that handles both non-linearity and non-stationarity will be presented in Chapter 4.

Chapter 4

Empirical Mode Decomposition

A method that handles both non-linearity and non-stationarity is the *Empirical Mode Decomposition* (EMD). This method was pinoeered by Norden E. Huang et al. [3] in 1998 as an adaptive time-series method. It assumes that any oscillatory time-series consists of different modes of oscillation, called intrinsic mode functions (IMFs). The purpose of the method is to identify the IMF functions by their characteristic time scales, and then decompose the data according to this. If this method is combined with Hilbert spectral analysis, it is called *Hilbert - Huang Transform* (HHT).

In this chapter, the working principle of the EMD method will be explained and some drawbacks and extensions of the method will be presented.

4.1 Intrinsic Mode Functions

As mentioned, the EMD decomposes a signal into IMFs, and in this section, the properties of an IMF will be explained. An IMF is a function that fulfils the following two conditions [3] :

1. For the whole data set, the number of extrema and zero crossings are equal or differ at most by one;
2. At any point, the mean of the local maxima envelope and the local minima envelope is approximately zero.

The first condition is not a new idea, and such principle is not only used the EMD method. For a Gaussian process, this is similar to the narrow band requirements. The second one is, on the other hand a new idea. Other methods, e.g., Fourier analysis, are based on global requirements, but EMD is based on a local requirement. Such local requirements avoid

unwanted fluctations induced by asymmetric wave forms in the instantaneous frequency [3].

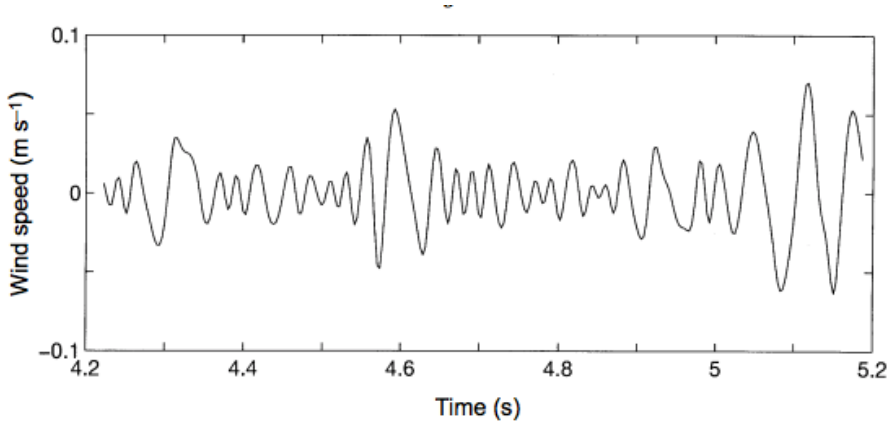

Figure 4.1: A typical IMF with same number of extrema and zero crossings. It also shows symmetry in the upper envelope (defined by the maxima) and the lower envelope (defined by the minima), with respect to zero [3].

4.2 Empirical Mode Decomposition - Algorithm

The purpose of the EMD method is to empirically identify the intrinsic oscillatory modes and decompose the data. This is done through a process called *sifting*. The algorithm considers signal oscillations at a highly local level and separates the data into time scale components which are local and non-overlapping [3]. Thus, the EMD decomposes a oscillatory signal into IMFs.

The data set x_t is decomposed into IMFs $x_n(t)$ and a residue $r(t)$ such that the signal can be expressed as:

$$x(t) = \sum_n x_n(t) + r(t) \tag{4.1}$$

The sifting process consists of the following steps, which are also illustrated in Figure 4.2:

- Step 1: Initialize the following: n:= 1, $r_0(t) = x(t)$
- Step 2: Extract the IMFs as follows:
  1. Set $h_0(t) = r_{n-1}(t)$ and $k = 1$
  2. Identify all the local maxima and minima of $h_{k-1}(t)$.

3. By cubic splines interpolation, construct the upper and lower envelopes for $h_{k-1}(t)$. The upper envelope, $U_{k-1}(t)$, is defined but the local maxima and the lower envelope,$L_{k-1}(t)$ is defined by the local minima.

4. Determine the mean, $m_{k-1}(t)$ = 1/2($U_{k-1}(t) - L_{k-1}(t)$) of both the upper and lower envelopes.

5. Compute the k^{th} component: $h_k(t) = h_{k-1}(t) - m_{k-1}(t)$.

   (a) If $h_k(t)$ does not fulfil the criteria set for an IMF, the k must be increased to $k + 1$. Go back to step 2,2.

   (b) If $h_k(t)$ fulfils the criteria set for an IMF, then set $x_(n)(t) = h_k(t)$ and $r_n(t) = r_{n-1}(t) - x_n(t)$.

- Step 3: Stop the sifting process if $r_n(t)$ is a residue. If it is not a residue, increase n to $n + 1$ and start over at step 2 again.

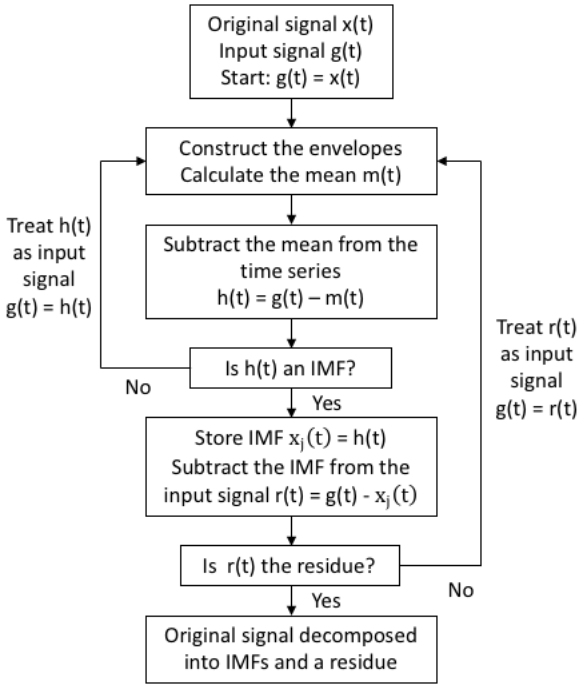

Figure 4.2: Flow diagram of the EMD algorithm [23].

4.3 Drawbacks of EMD

Even though there are many benefits to the EMD, there are some aspects that must be considered and noticed. The method does have some drawbacks which will be presented in this section. The drawbacks are gathered from [23], except for the concept *mode mixing*, which is from [24, 25, 26, 27].

4.3.1 Mode mixing

When EMD is applied there is a risk of mode mixing. Mode mixing is when different modes of oscillations coexist in a single IMF, and the concept was pointed out by Huang in 1998 [27]. Mode mixing can occur, for example, when the data contains frequencies that are close or the data exhibit intermittency. This causes the IMFs to lose its physical meaning and hampers the analysis. To illustrate the concept of mode mixing the the decomposition of the following signal *x(t)* can be considered:

$$x(t) = \begin{cases} \sin(2\pi f_1 t) + \sin(2\pi f_2 t), & \frac{1}{30} \leq t \leq \frac{2}{30}, \\ \sin(2\pi f_1 t), & \text{otherwise.} \end{cases} \tag{4.2}$$

The decomposition of the signal *x(t)* is illustrated in Figure 4.3.

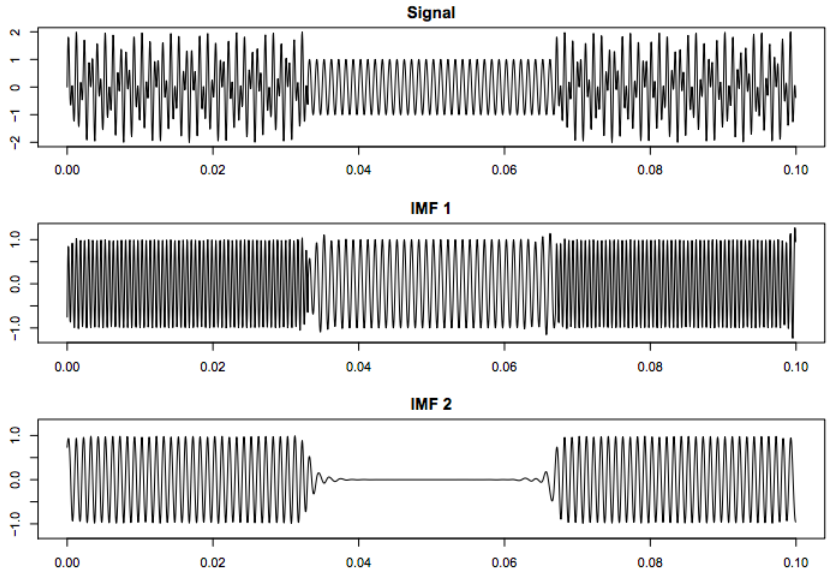

Figure 4.3: Illustration of a signal, *x(t)*, that is decomposed using EMD and where mode mixing occurs. The signal consist of two sine curves with frequencies f_1 = 1776 Hz and f_2 = 1000 Hz. The mode mixing is visible in the span $t = \frac{1}{30}$ and $t = \frac{2}{30}$ [27].

The decomposition illustrated in Figure 4.3 show that in the time span $t = \frac{1}{30}$ and $t = \frac{2}{30}$, IMF 1 absorbs the component that appears in IMF 2. Thus, the decomposition of this signal is influenced by mode mixing. As illustrated by this example, mode mixing can be a problem when EMD is applied to a signal. There are different methods available for avoiding mode mixing when applying EMD, and some of them can be seen in [24, 25, 26].

4.3.2 Estimating envelopes

The most used technique for estimation of the upper and lower envelopes, which are needed to identify the mean at every time point, is the *spline interpolation*. The splines represent functions which are piece wise composed from polynomials of order n. In order to locate the extrema precisely, *over-sampling* can be used. Of a time series $x(t)$, cubic splines are often used to interpolate maxima and minima. In general, they give proper results, but they come with a computational cost. There are alternative schemes for interpolation that has been proposed using *taut* or *rational* splines. These methods allow, depending on another parameter, a smooth transition between a linear and a cubic spline [28]. In addition, there are other techniques available, and it has also been attempted to estimate local means directly and not use envelopes at all (see [29],[30]). Anyhow, in order to get proper results when using an algorithm that uses envelopes, the envelopes must be properly estimated.

4.3.3 Stopping criterion

Unless otherwise specified, standard EMD continues the sifting process on the full signal until it no longer exist local segments. This can cause *oversampling* and splitting of IMFs into fragments that are meaningless. A solution to this is to set a stopping criterion. One possibility is to specify the number of siftings. Another possibility is to use a criterion, called the Rilling stopping criterion, that is based on the total variance:

$$\sigma_i^2 = \sum_{n=0}^{N} \frac{(h_{i,k-1}(t_n) - h_{i,k}(t_n))^2}{h_{i,k-1}(t_n)} \tag{4.3}$$

The IMFs are obtained when $\sigma_i^2 < \delta$ holds for some chosen threshold δ. The procedure will stop when the residue $r_n(t)$ is either a constant or a monotonic slope that only contains one extrema. Another stopping criterion can be used. This is an evaluation function that has been introduced by [31]:

$$\sigma(t) = \frac{U(t) + L(t)}{U(t) - L(t)} \tag{4.4}$$

which uses two thresholds δ_1 and δ_2. The sifting process iterates until $\sigma(t) < \delta_1$ for a prescribed fraction (1-α) of the total duration and $\sigma(t) < \delta_2$ for the rest. This method

introduces three new parameters that the user has to set. If these parameters are not chosen correctly, it might have impact on the IMFs.

4.3.4 Boundary conditions

When spline interpolation are used, fluctuations in the beginning and the end of the data set occur. If the first and last point are considered as knots of the upper and lower envelopes, then results that do not have physical meaning occur. As illustrated in Figure 4.4, these defects will propagate to the signal components that are extracted later on. There are a number of solutions to this, for example, padding the ends with typical waves [3], mirroring the extrema closest to the ends [31] or by using the average of the two closest for the maximum or minimum spline [32].

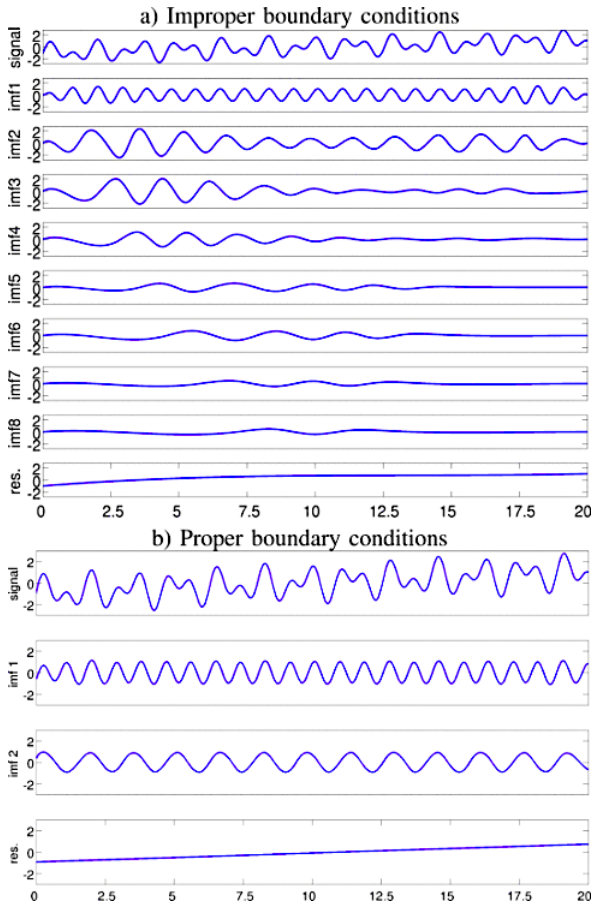

Figure 4.4: a) EMD of the non-stationary time series $x(t)$ = sin(7t)+sin(4t)+0.1t-1, where the first and last data point of the time series are treated as knots of *x(t)*, which leads to improper boundary conditions. b) EMD of the same non-stationary time-series with proper boundary conditions [23].

By comparing the results illustrated in Figure 4.4 a and b, the effect of not choosing the proper boundary conditions is clearly visible. In Figure 4.4 a, the last data point of the time series have been treated as knots of *x(t)*. This leads to an end effect for each of the IMFs, revealing distorted results at both of the ends. For each new IMF that is extracted the end effects are influencing a larger part of the IMF. In addition to the end effects, the oscillating modes of the signal is not extracted correctly by either of the IMFs. When the boundary conditions are chosen properly, the oscillating modes are extracted properly, as seen in Figure 4.4 b.

4.4 Extensions of EMD

The EMD is an analysis method which is applied to the full length signal. If the signal is long, there is a need for large computer memory and this can limit the method. This also means that the method is not suited for analysis of data streams. If the method was able to analyse data streams, it would provide more opportunities and would be beneficial for real-time analysis. Such an extension of this method, called Online EMD, allows the analysis of data streams and will be presented in Chapter 5. In this section other extensions will be discussed briefly.

4.4.1 Local EMD

In the standard EMD, the iteration process is continued as long as there is a *local zone* where the mean of the envelopes is not considered as too small. As mentioned in section 4.3, over-iterating on the whole signal to achieve a better local approximation can result in pollution of other parts of the signal. This pollution is in particular uniformizing the amplitude and in over-decomposing it by spreading its components out over adjacent modes. In [31] a variation of the EMD, called local EMD, is described. This method introduces another step in the sifting process. In comparison to the standard EMD, this method identifies the local zones where the error remains large and isolates them. Then, extra iterations are applied to only them. In order to achieve this, a weighting function $\omega(t)$ is introduced and applied where sifting is still necessary. This can be implemented into the EMD algorithm like this:

$$h_{j,n}(t) = h_{j,n-1}(t) - \omega_{j,n}(t)m_{j,n}(t) \tag{4.5}$$

This can be used to improve the sifting process and avoide *over-sifting*.

4.4.2 Ensemble EMD

Ensemble EMD (EEMD) is method is a noise assisted method that is presented in [33]. In [23] it is stated that method considers true IMFs to an ensemble average of extracted IMFs according to

$$x_j = \frac{1}{N} \sum_{i=1}^{N} x_{ji}(t) \tag{4.6}$$

where white noise with finite amplitude, constant variance and zero mean is added to the time-series $x(t)$. The mean IMFs will stay within the natural dyadic filter windows, and thus, reduce the possibility of mode mixing and keep the dyadic property.

The working principle of EEMD can be summarized by the following steps [33]:

1. Add a white noise series to the data;
2. Decompose the data with the added white noise into IMFs;
3. Repeat step 1 and step 2 over and over again with different white noise series;
4. Calculate the ensemble means of the IMFs as the final result.

The added white noise will cancel each other out in the final mean of the IMF. To illustrate the performance of EEMD an example is given in [23]. Here, the performance of EEMD vs EMD is compared. The result can be seen in Figure 4.5. In this example, two signals ($x_1(t) = 0.1\sin(20t)$ and $x_2(t) = \sin(t)$) are superimposed, where signal $x_1(t)$ is interrupted for a certain time span. The EEMD applied by using an ensemble of 15 different noisy signals.

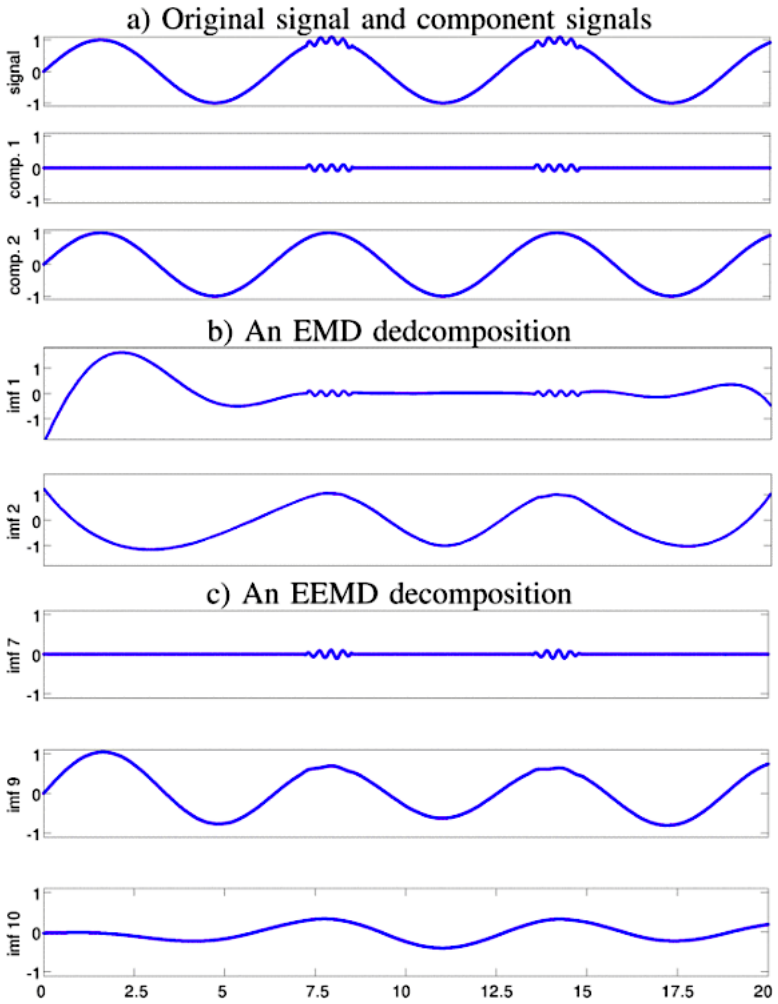

Figure 4.5: a) Superposition of the signals $x(t) = x_1(t) + x_2(t)$ = 0.1sin(20t)+sin(t) and the component signals. b) IMF 1 and IMF 2 obtained from EMD of the same signal. c) IMFs obtained by EEMD of the same signal using an ensemble of 15 different noisy signals [23].

The results obtained in Figure 4.5, reveals that the the EEMD provides a decomposition that is more accurate than the decomposition obtained using EMD for this specific signal. IMF 1 obtained with EMD should only consist of one of the two components, but as illustrated, it is clearly influenced by mode mixing as both of the components are present in the IMF. The EEMD on the other hand is able to extract the oscillating modes more accurate and is not influenced by mode mixing.

4.4.3 SEMD and wSEMD

The standard EMD is applied over the entire signal. Because of this, the method is limited by the computer memory which limits size of the time-series to be analyzed. Another issue is that the EMD cannot be applied online. Two Online version of EMD called *Sliding Empirical Mode Decomposition* (SEMD) and *Weighted Sliding Empirical Mode Decomposition* (wSEMD) are presented in [34]. SEMD decomposes a time-series of arbitrary length into a residue and IMF-like functions called *sliding intrinsic mode functions* (SIMFs). SEMD uses a window, with fixed size *m*, and a step size *k*, which has to be chosen. Within this window, EMD or EEMD is applied. Then, the window is shifted by *k* samples and EMD is applied again. The step size *k* should be chosen much smaller than the size *m* to avoid discontinuities. If $k < m$ and the window size is a multiple of the step size, i.e. if

$$E = \frac{m}{k} \in \mathcal{N} \tag{4.7}$$

holds, then for each sample *x(t)* of the original signal time series, *E* estimates are calculated within the different windows m_i, as soon as the first *E* iterations have been done. The time series in each segment m_i is decomposed by EMD into *j* different IMFs $x_{m_i j}(t)$ and a local residue $r_{m_i}(t)$ according to

$$x_{m_i}(t) = \sum_j x_{m_i j}(t) + r_{m_i}(t), \tag{4.8}$$

where the number of sifting is kept equal for all segments. The resulting IMFs are gathered in a matrix with corresponding sample points. Columns that corresponds to the beginning or the end of the time series are left out from further processing as they are deficient. This assures that all columns have the same amount of information for estimating the average of IMF amplitudes at each time point *t* in each segment. This finally yields for $t > m$:

$$x_j = \frac{1}{E} \sum_i^{i+E-1} x_{m_i j}(t), \tag{4.9}$$

$$r(t) = \frac{1}{E} \sum_i^{i+E-1} r_{m_i}(t), \tag{4.10}$$

$$i = \left(\frac{t-m}{k}\right) + 2 \tag{4.11}$$

The resulting functions $x_j(t)$ are SIMFs and $r(t)$ is the residue. To summarize, equations (4.9) - (4.11) describes the SEMD decomposition process and a schema of the SEMD algorithm is illustrated in 4.6.

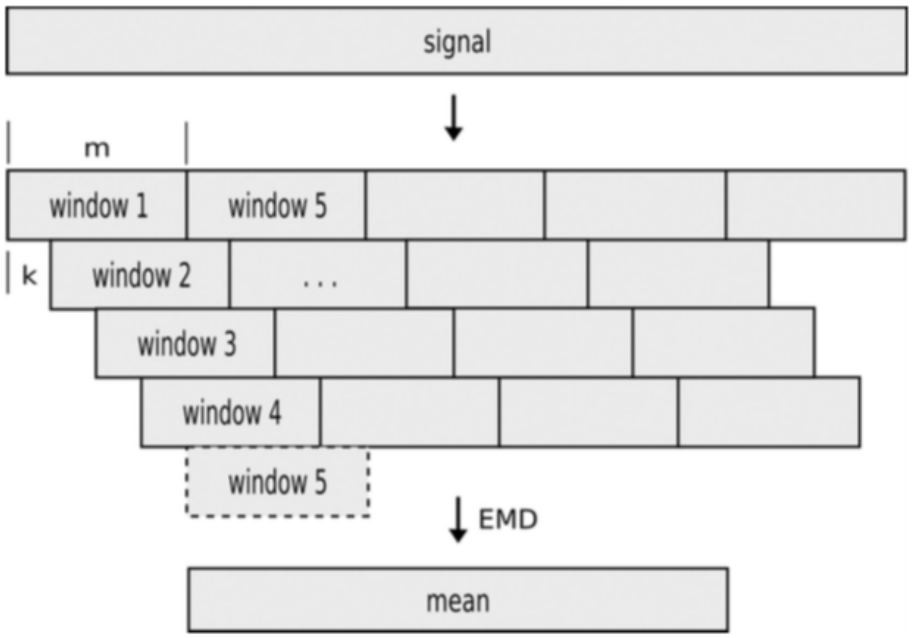

Figure 4.6: Scheme of the SEMD algorithm. The time-series segments in the shifted windows are EEMD. IMFs and the residue are determined by mode amplitudes which are averaged over corresponding samples in all windows. *m* is the window size and *k* is the step size [34].

The end-effects of the standard EMD are reduced when using SEMD. However, estimates that comes from the boundaries are expected to be more defective compared to the ones from the middle part of any specific window. In order to solve this, a weighted sum of the estimates can be used. To accomplish this, the resulting IMFs and residue are multiplied by a vector of rank *m* for every window,

$$w(n) = exp\Big(-\frac{1}{2}\big(\alpha\frac{2n}{N}\big)^2\Big), \tag{4.12}$$

$$-\frac{N}{2} \leq n \leq \frac{N}{2}, \quad \alpha = 2.5, \quad N = m - 1 \tag{4.13}$$

In order to calculate the data point of an IMF, the first step is to calculate the sum over *n* estimates multiplied by *n* weighting coefficients. After this, the resulting sum is normalized by the reciprocal of the sum of all used weights again. Then, the amplitude and the sliding residue is preserved and the completeness of the decomposition is obtained again. If this described weighting is used, the method is called wSEMD.

Chapter 5

Online EMD

In this chapter an extended version of the EMD called Online EMD will be presented. The Online EMD will also be used to analyze data later on. The algorithm and description of this method is from [5].

Chapter 4 described several advantages of applying EMD. However, there are some drawbacks as well:

1. The classical EMD is not able to analyze real time data.
2. The classical EMD requires increasing computational resources to analyze a growing data.
3. The classical EMD converges in a number of sifting steps that increases for long data, which causes over-sifting issues.

The reasons above are namely because each sifting step considers the entire data span. A solution to these problems is to process the signal in blocks. However, there is an issue when merging the IMFs from two sequential blocks. When merging these IMFs, there may be discontinuities due to the boarder effect of the EMD. A solution to this is to apply EMD on overlapping blocks, and hence, prevent discontinuities by merging the results with a smoothing function, like the wSEMD described in section 4.4.3. This method restrains a constant number of sifting steps and IMFs for all analyzed blocks, which prevents blocks with discordant number of IMFs. The Online EMD that will be presented here takes advantage of the sliding approach of wSEMD. This new method has low computational and low memory requirements like the wSEMD while retaining the essence of EMD. A great advantage of the Online EMD is that it does not require any prior knowledge about the number of underlying components in a set of data or the sifting steps that are required to extract them. In the following section, the algorithm for the Online EMD will be presented.

5.1 Algorithm of online EMD

Online EMD uses a sliding window that includes l local extrema to monitor data. The window is shifted by one extremum and the fastest oscillation is extracted using standard EMD. After the fastest oscillation is extracted, a stitching procedure stitches the modes of this window to the previous extracted modes that overlap in the current window. According to the windows position in time, the stitching procedure weights the overlapping modes from different windows and then averages them. The window function for the stitching procedure is $\tilde{\phi}(s)$ on $[-\tau, \tau]$ and zero outside, e.g., $\tilde{\phi}(s) = \frac{1}{\sqrt{2\pi}}\exp(-\frac{s^2}{2})$ - $\frac{1}{\sqrt{2\pi}}\exp(-\frac{\tau^2}{2})$, with $\tau = 3$, that restrain discontinuities from boundary errors [5]. The stitching procedure causes the algorithm to gradually discover data for the first IMF and the residual. Other IMFs are discorvered by repeating the analysis with the residual as the input signal. The stitching procedure is illustrated in Figure 5.1.

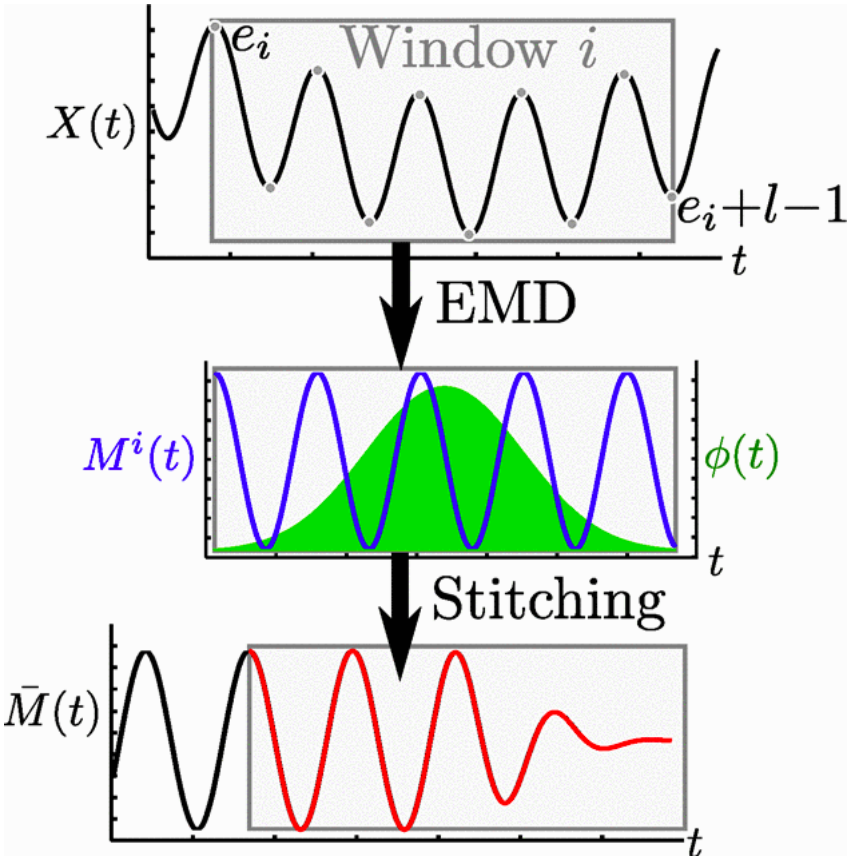

Figure 5.1: An overview of the online EMD sliding window and the stitching procedure. The window includes $l = 10$ extrema. Using classical EMD, the fastest oscillation, M^i in blue, is extracted and the window function, ϕ, is plotted in green. The weighted IMF, $\hat{M}^i$, stitched to the previous uncovered IMFs in red [5].

The online EMD algorithm is as follows [5]:

1. Initialize *i* = 1, $\Phi^0(t) = 0$, $e_1 = 0$ the starting time of the signal and $\bar{M} = 0$.
2. Identify the window starting at e_i containing *l* consecutive local extrema (e_1,...,e_l) of the signal *X(t)*.
3. Using classical EMD, extract the first IMF (i.e. fastest oscillation) $M^i(t)$ of the data in the window.
4. Let $e_1^{'}$,...,$e_l^{'}$ be the positions of the $l^{'}$ extrema in M^i. Set s_k = -τ + 2(*k*-1)τ/($l^{'}$-1) for $k \in 1,...,l^{'}$. We define warped weights ϕ_k(t) for $k \in 1,...,l^{'} - 1$ and $t \in [e_k^{'},...,e_{k+1}^{'}]$ as:
$$\phi_k(t) = \tilde{\phi}\left(s_k + (s_{k+1} - s_k)\frac{t - e_k^{'}}{e_{k+1}^{'} - e_k^{'}}\right) \tag{5.1}$$
(and 0 outside). The weighted IMF $\hat{M}^i$ is defined as:
$$\hat{M}^i(t) = (\phi_1(t)M_1^i(t), ..., \phi_{l'-1}(t)M_{l'-1}(t))$$
where M_k^i(t) is the mode between two extrema:
$$M_k^i(t) = M^i(t), \qquad e_k^{'} \leq t < e_{k+1}^{'} \tag{5.2}$$
The total of weights is kept in memory:
$$\Phi^i(t) = \Phi^{i-1}(t) + \sum_{k=1}^{l^{'}-1} \phi_k(t) \tag{5.3}$$
5. Stitch $\hat{M}^i$ on the weighted IMFs already extracted:
$$\bar{M} = \bar{M} + \hat{M}^i \tag{5.4}$$
and normalize the part of the data that will go out of the sliding window at the next iteration:
$$\bar{M}(t) = \bar{M}(t)/\Phi^i(t) \quad \text{for all} \quad t \in [e_i, e_{i+1}] \tag{5.5}$$
6. This newly finalized part of the IMF $\bar{M}(t)$, for t $\in [e_i,e_{i+1}]$ is subtracted from the data,
$$R^i = X^i(t) - \bar{M}(t) \quad \text{for all} \quad t \in [e_i, e_{i+1}] \tag{5.6}$$
The resulting data R^i is pushed to another instance of online EMD in order to identify subsequent IMFs.
7. Increase *i* to *i+1* and go back to step 2.

There are some remarks to this online EMD algorithm:

1. The head of the stitched IMF, $\bar{M}(t)$, $e_{i+1} \leq t \leq e_{i+l-1}$, needs subsequent data to the completed, thus, the IMFs uncovered by online EMD feature a lag $e_{i+l-1} - e_i < \Delta t < e_{i+l} - e_i$. As the value of Δt depends on the distances between the extrema, IMFs with lower frequencies exhibit longer lags.

2. For the stitching procedure of steps 4 and 5, the number of extrema $l^{'}$ of the IMF is possibly different from the number of extrema l that defines the sliding window; it occurs in (rare) situation where small fast oscillations are added to large slow oscillations. It can happen that some extrema of the fast oscillations do not lead to extrema in the combined signal - yet they can be recovered by EMD that will create new extrema in the extracted IMF. This is why this distinction is done between l and $l^{'}$.

5.2 Execution time

In comparison to the classical EMD, the online EMD has the possibility to analyze data streams. This is a great advantage and opens doors for other applications. To demonstrate this, both the standard EMD and the online EMD are used in [5] to analyze a sinusoid with a monotonic function, and a white noise signal, both including 280k samples. These signals are analyzed in a streaming fashion. This means that the signals are split into batches, in this case 10k samples, that are sequentially analyzed. The classical EMD has a disadvantage compared to the online EMD. For each new batch, the standard EMD must process the previous batches with the new one. This causes a longer execution time for each batch, and the execution growth rate depends on the number of undiscovered IMFs. Figure 5.2 shows the execution time of the online EMD and standard EMD for the sinusoidal signal. It can be seen that the last execution time of the last batch for the standard EMD is four times longer than for the first batch. Looking at the same signal, but for the standard EMD of the white noise, the execution time of the last batch is about 10^4 higher than the execution time for the first batch. The execution time for the online EMD also depends on the uncovered IMFs, but in comparison to the standard EMD, the computational cost is more stable. The online EMD is slower to analyze each batch because of the sliding window and the stitching procedure. However, the online EMD has almost constant execution time for each batch. This makes this method advantageous for analyzing data streams with an increasing number of oscillatory components. The comparison of the classical EMD and the online EMD can be seen in figure 5.2, where both of the methods uses the Rilling stopping criterion.

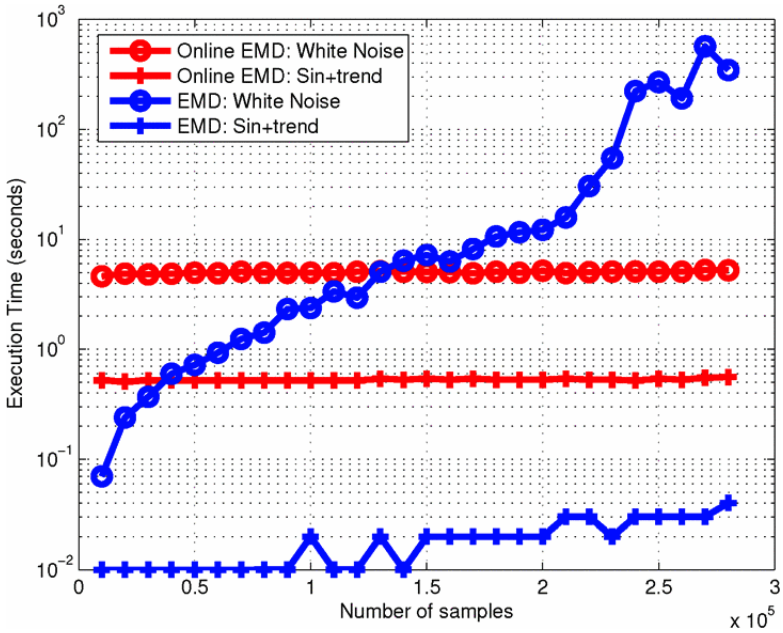

Figure 5.2: Execution time of online EMD ($l = 20$) and classical EMD (both using Rilling stopping criterion) with a white noise signal and a sinusoid with a trend. [5]

Chapter 6

Hilbert transform and Instantaneous frequency

The combination of EMD and Hilbert Transform is called as mentioned called HHT [3]. In this chapter, the Hilbert transform and an algorithm for calculating the instantaneous frequency will be presented. When analyzing signals that contain harmonic components it is important to find at which order they occur. Therefore, it is important to calculate the instantaneous frequency. The first step after the IMFs have been extracted is to use the Hilbert transform to form the analytical signal, and then apply an algorithm for calculating the instantaneous frequency.

6.1 Hilbert transform

The advantages of using the Hilbert transform (HT) can be listed as below [35]:

- The HT can give the amplitude and instantaneous frequency of a measured signal, and hence solves a typical demodulation problem.
- In comparison to the Fourier analysis, which assumes that a signal is a sum of a number of sine waves, the HT allows a complex demodulation analysis of the form of a single but modulated sine wave.

The Hilbert transform is a integral transform, like Laplace and Fourier, and it is named after David Hilbert [35]. The HT of a function $x(t)$ is defined by an integral transform as follows:

$$H[x(t)] = \tilde{x}(t) = \pi^{-1} \int_{-\infty}^{\infty} \frac{x(\tau)}{t-\tau} d\tau \tag{6.1}$$

The mathematical definition in the above equation does not give much understanding of the HT. However, physically, the HT gives a better understanding of what the transformation does. Physically, the HT can be seen as a linear filter that does not change the amplitudes of the spectral components, but the phases are shifted by $\pi/2$. This shifting can be seen in Figure 6.1 c. The HT representation $\tilde{x}(t)$ of the original function is the convolution integral of $x(t)$ with $((\pi t)^{-1})$, and it is written as $\tilde{x}(t) = x(t) * (\pi t)^{-1}$. In Figure 6.1 a the impulse response function of the ideal HT can be seen, and in Figure 6.1 b and 6.1 c the module and phase characteristics are shown.

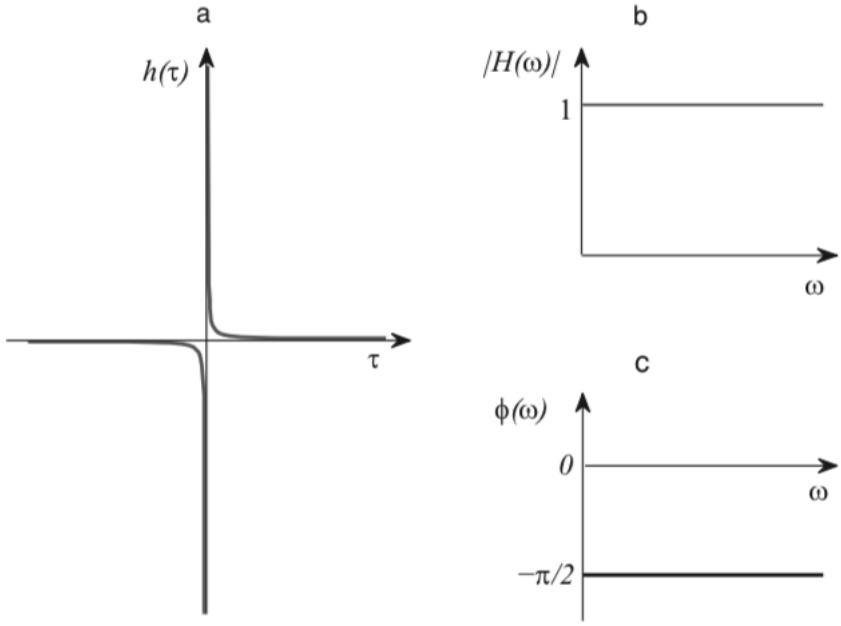

Figure 6.1: The ideal HT: the impulse response function (a), the module (b) and the phase (c) of the HT function [35].

This means that when HT to is applied to a constant, it returns zero. If HT is applied twice to a function, the result is the original signal, but with opposite sign. If the HT is applied four times to a real function, it returns the original function. This means that a function and its HT are orthogonal over an infinite interval.

6.2 Instantaneous frequency

For non-stationary signals, where the spectral characteristics vary with time, the instantaneous frequency is an important concept. For these signals, the instantaneous frequency is a time varying parameter that defines the location of the spectral peak of the signal as it varies with time.

The instantaneous angular frequency, as indicated by equation (6.2), is the first derivative of the instantaneous phase as a function of time and it plays an important role in signal analysis. At any given time, there is a single value of instantaneous phase [35].

$$\omega(t) = \dot{\psi}(t) \tag{6.2}$$

where $\dot{\psi(t)}$ = arctan($\tilde{x}(t)/x(t)$)

The angular frequency is given in radians per second, while the cycle frequency is given in Hertz. To avoid unwrapping of the phase, the instantaneous frequency can be calculated as:

$$\omega(t) = \frac{x(t)\dot{\tilde{x}}(t) - \dot{x}(t)\tilde{x}(t)}{A^2(t)} = \text{Im}\left[\frac{\dot{X}(t)}{X(t)}\right] \tag{6.3}$$

where A(t) = $(x^2(t)+\tilde{x}^2(t)))^{1/2}$

The instantaneous frequency measures the direction and rate of a phasor rotation in the complex plane.

6.2.1 Algorithm for calculating instantaneous frequency

There are several algorithms available for calculating the instantaneous frequency. The one that will be presented here is an algorithm without derivation. If the calculation of the instantaneous frequency is based on the derivative of angles, there might be some challenges. If the signal (IMF in the context of EMD) is not clean, the results will become very noisy. Thus, it is an advantage to do this calculation without the derivative. The algorithm is from [35] but some alterations have been made by Prof. Olav Bjarte Fosso at the Department of Electric Power Engineering, NTNU. The algorithm is easy to implement and it takes into account the discrete form of a real signal $x(n)$ that is obtained by sampling the analog signal at discrete instants of time t_n. The analytical signal will be on the form $X_n = x_n + i\tilde{x}_n$.

Using the trigonometric property:

$$\arctan x - \arctan y = \arctan\left(\frac{x-y}{1+xy}\right) \tag{6.4}$$

The difference in angle is then:

$$\begin{aligned}\Delta\Psi_n &= \Psi_{n+1} - \Psi_n \\ &= \arctan\left(\frac{x^h_{n+1}}{x_{n+1}}\right) - \arctan\left(\frac{x^h_n}{x_n}\right) \\ &= \arctan\left(\frac{\frac{x^h_{n+1}}{x_{n+1}} - \frac{x^h_n}{x_n}}{1 + \frac{x^h_{n+1}x^h_n}{x_{n+1}x_n}}\right) \\ &= \arctan\left(\frac{x^h_{n+1}x_n - x^h_n x_{n+1}}{x_{n+1}x_n + x^h_{n+1}x^h_n}\right)\end{aligned} \tag{6.5}$$

The multiplication of the initial analytic signal and the complex conjugate produces a new complex function:

$$\begin{aligned}X_n X^*_{n+1} &= (x_n + ix^h_n)(x_{n+1} - ix^h_{n+1}) \\ &= x_n x_{n+1} + x^h_n x^h_{n+1} + i(x^h_n x_{n+1} - x_n x^h_{n+1})\end{aligned} \tag{6.6}$$

$$\omega = \frac{\Delta\psi}{\Delta t} = \frac{\arctan(-X_n X^h_{n+1})}{\Delta t} \tag{6.7}$$

$$f = \frac{1}{2\pi}\frac{\Delta\psi}{\Delta t} = \frac{\arctan(-X_n X^*_{n+1})}{\Delta t} \tag{6.8}$$

This algorithm does not require any unwrapping of the phase and it is less sensitive to noise.

Chapter 7

Results and discussion

In this chapter, analysis using both the standard EMD and the online EMD will be presented. The purpose of the analysis is to examine the decomposition provided by both the standard EMD and the online EMD for harmonic signals. The standard EMD is applied using both a Python implementation and a MATLAB implementation of the method. The standard EMD applied in MATLAB is the same standard EMD the online EMD applies in the shifting window. Hence, it is useful to apply the standard EMD and the online EMD in order to have a basis of comparison.

The analysis is divided into three parts. In the first part, a real current measurement with fundamental frequency of 60 Hz, illustrated in Figure 7.1, and an elongated signal, illustrated in Figure 7.2, is analyzed using the standard EMD implemented in Python. The real current measurement is from [36], and was provided by Jalal Khodaparast Ghadikolaei, a postdoctoral researcher at the Department of Electric Power Engineering, NTNU. The original signal is 0.05 seconds long, and has only 6 extrema. Following [5], in order to avoid errors introduced by the stitching window, a minimum number of 10 extrema is required to apply the online EMD. Thus, the original signal was extended. The elongated signal is a duplication of the real current measurement, and it is duplicated 27 times, making it 1.35 seconds long. In the second part, the same two signals, the original current measurement and the elongated signal, are analyzed using the standard EMD implemented in MATLAB. Finally, in the third part, the online EMD is applied to the elongated signal.

There are several ways to implement the EMD in both MATLAB and Python. In this analysis, one implementation of the EMD in MATLAB and one implementation in Python are applied and compared.

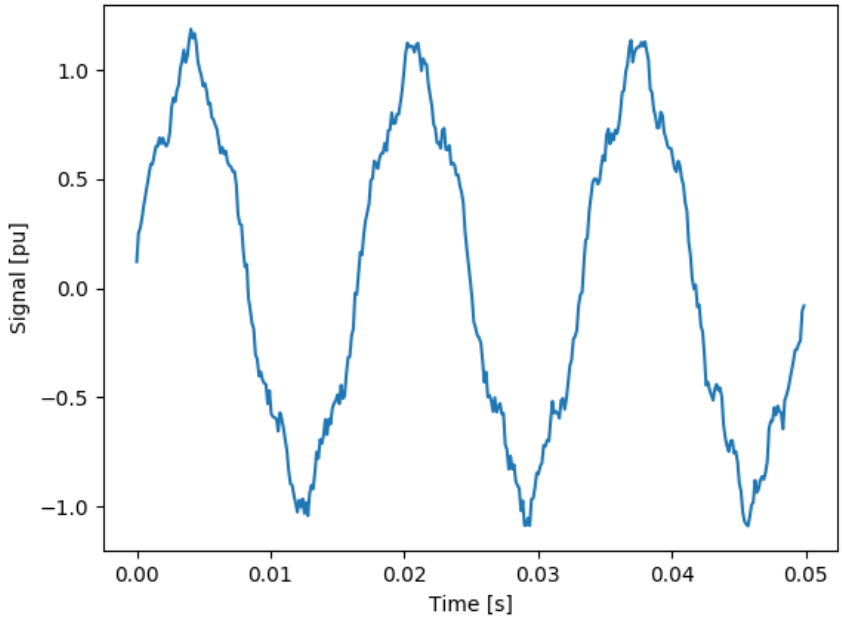

Figure 7.1: Real measurement of a current containing harmonics.

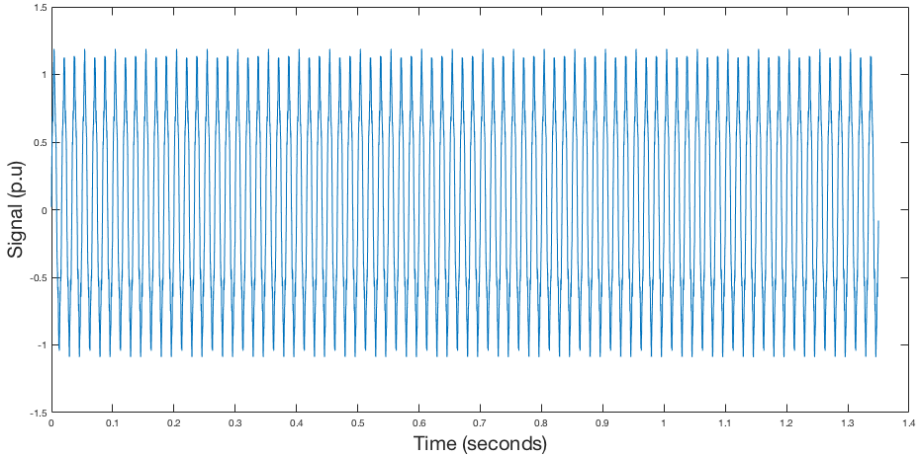

Figure 7.2: Duplicated signal of the current measurement in Figure 7.1.

7.1 Part 1 - Analysis using the standard EMD (Python code)

In this section, the standard EMD will be applied to both the original current measurement in Figure 7.1 and the duplicated signal in Figure 7.2 using Python. After EMD is applied, and the decomposition is obtained, the frequencies of the signal is calculated using both instantaneous frequency and FFT.

7.1.1 Original current signal

The current measurement has been analyzed previously in [11] using a code implemented in Python, and the main results from this analysis will be presented here. The analysis was performed using 23 siftings as the stopping criteria as this provided the most accurate decomposition. The decomposition using the standard EMD is illustrated in Figure 7.3.

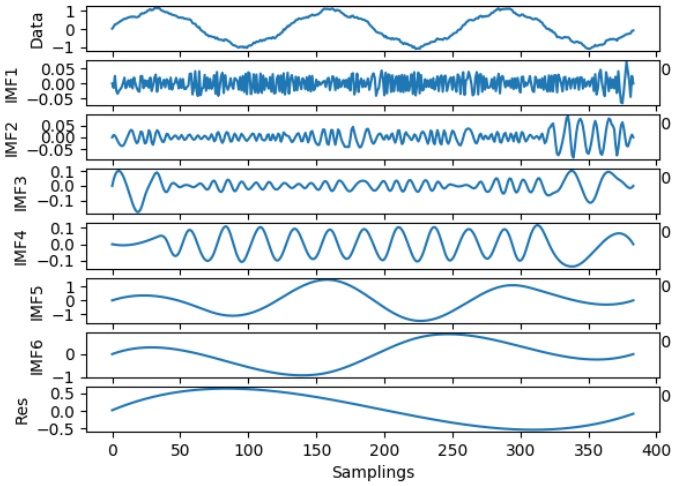

Figure 7.3: Standard EMD of the original current measurement. The first plot is the data, the following 6 plots are the IMFs and the last one is the residue. The standard EMD is performed using 23 siftings.

In the frequency result in Figure 7.3, the first two IMFs, IMF 1 and IMF 2, are noise, and IMF 3, IMF 4 and IMF 5 carry information about the frequency components of the measurement. The IMFs are distorted at the ends, making it clear that the decomposition suffers from end effects. The end effects propagate as the number of IMFs that are extracted increases, making IMF 5 more influenced by the end effects than IMF 3. In addition to the instantaneous frequency of the IMFs, the FFT of the signal is calculated in order to verify the frequency results. The frequency results are illustrated in Figure 7.4.

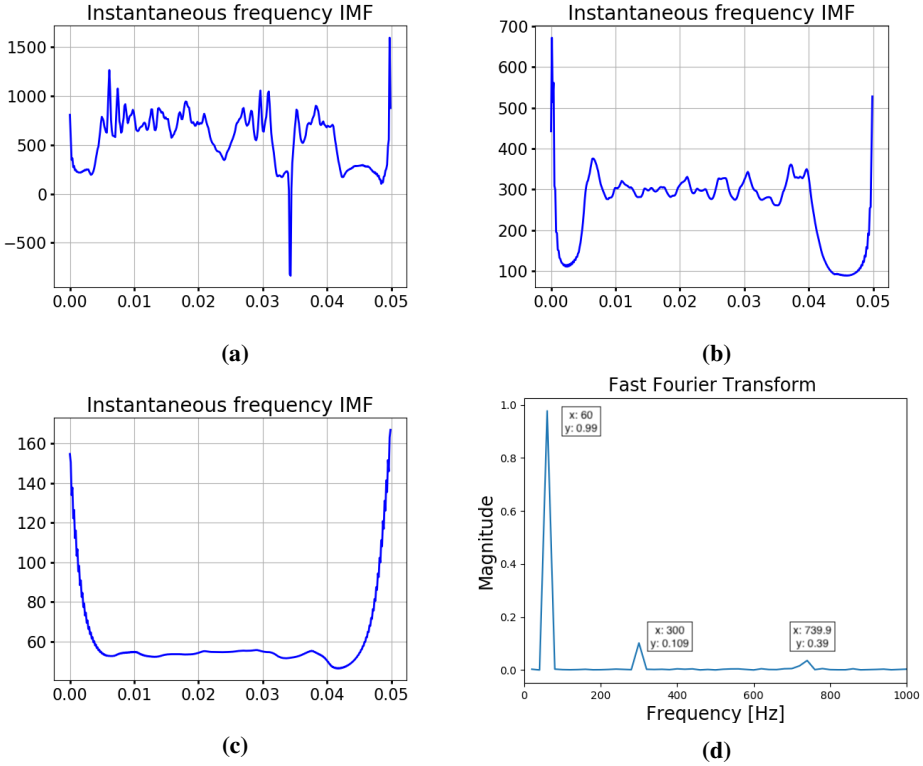

Figure 7.4: a) Instantaneous frequency of IMF 3, b) instantaneous frequency of IMF 4, c) instantaneous frequency of IMF 5 and d) FFT of the current measurement. In a, b, and c the frequency in Hertz on the y-axis and the time, in seconds, is on the x-axis.

In Figure 7.4 a, the instantaneous frequency of IMF 3 is presented. The result reveals a oscillating frequency mainly between 500 Hz and 1000 Hz. Just by this result, it is not possible to confirm that this is in fact the IMF that carries only the information about one of the harmonic components of the signal, and it might carry some noise as well. Even though this instantaneous frequency do not present an accurate result, the FFT result presented in Figure 7.4 d, reveals that the signal consist of a frequency component of approximately 740 Hz, which reinforces the instantaneous frequency result. The instantaneous frequency of IMF 4 on the other hand reveals a more constant frequency result at approximately 300 Hz. In the middle part, where the IMF is not influenced by end effects, there are small deviations, and a frequency of 300 Hz can be concluded as found. This is also verified by the FFT result in Figure 7.4 where a frequency component of 300 Hz is calculated. The instantaneous frequency of IMF 5 reveals an almost constant result of just below 60 Hz. The previous knowledge of the current measurement is that it has a fundamental frequency of 60 Hz, which does not correspond to the instantaneous frequency calculated for IMF 5. The cause of the deviation between the fundamental frequency and the instantaneous frequency calculated for IMF 5 may be the end effect. As seen in Figure 7.3, IMF 5 is

heavily influenced by end effects, leaving not a complete period to analyse. This can influence the instantaneous frequency and the result may be distorted. As for the instantaneous frequencies for IMF 3 and IMF 4, the instantaneous frequency of IMF 5 can be verified by the FFT results presented in Figure 7.4 d, which reveals a frequency of 60 Hz.

In order to verify that the calculated frequency components actually is the correct frequency components of the signal, a reconstruction of the signal, based on the calculated frequencies, is made and compared to the original signal. The frequency results reveal a 740 Hz, a 300 Hz and a 60 Hz component with amplitudes of approximately 0.04, 0.1 and 1 respectively. Hence, the reconstructed signal is composed as $\sin(2\pi 60t) + 0.1\sin(2\pi 300t) + 0.04\sin(2\pi 740t)$. The synthetic signal and the original signal is plotted together and the result is illustrated in Figure 7.5.

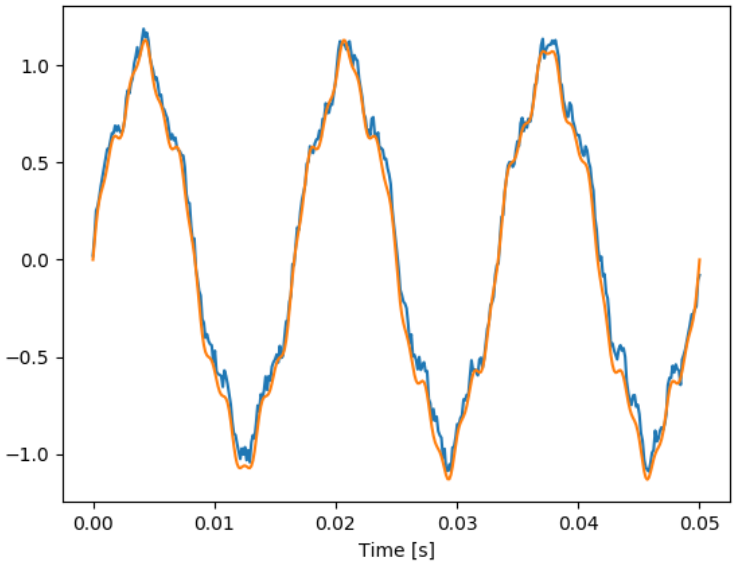

Figure 7.5: Original current measurement (in blue) and the reconstruction as $\sin(2\pi 60t) + 0.1\sin(2\pi 300t) + 0.04\sin(2\pi 740t)$ (in orange).

In Figure 7.5, the reconstruction (in orange) and the original signal (in blue) are plotted together. By comparing the two signals, there are some deviations that distinguish the two signals. Since the original signal is a real current measurement it is expected that it will contain some noise, and it seems to be the only thing that distinguishes the two signals. Based on the comparison of these two signals, and the frequency results in Figure 7.4, it can be concluded that the signal consist of a fundamental frequency of 60 Hz and the harmonic components of 300 Hz and 740 Hz.

7.1.2 Duplicated current signal

The duplicated current signal in Figure 7.2 was, as mentioned, constructed to make it suitable for the online EMD. It was chosen to analyze the duplicated signal with the standard EMD in Python as well in order to have a basis of comparison. The decomposition of the duplicated current signal using the standard EMD is illustrated in Figure 7.6. The standard EMD was applied to the duplicated signal with the same number of siftings as for the original signal, 23.

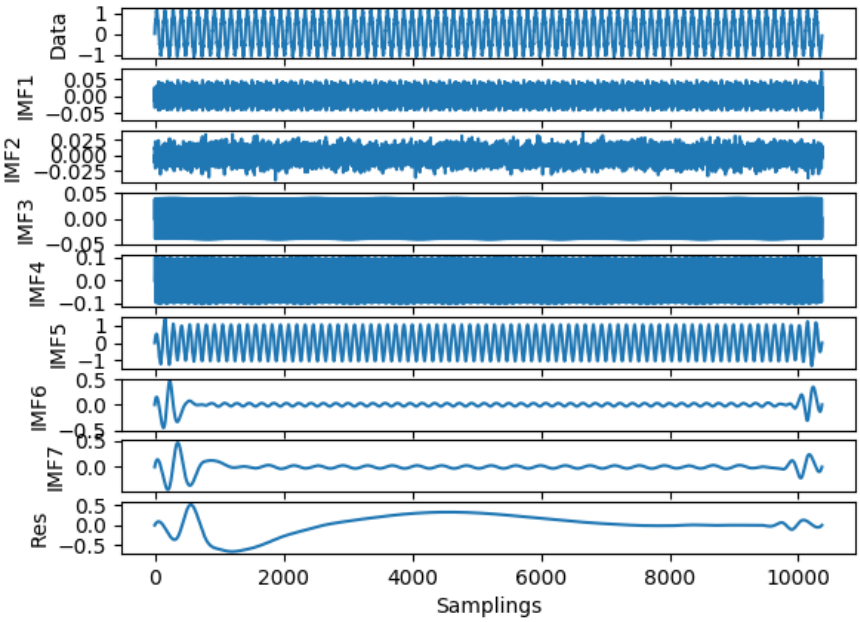

Figure 7.6: EMD of the duplicated current signal performed with 23 siftings.

Compared to the decomposition obtained for the original current signal in Figure 7.3, the decomposition obtained for the duplicated current signal is not as influenced by end effects. Since the duplicated signal is 27 times longer than the original signal, the end effects will not influence such a large part of the signal. This will provide a longer period where the IMF is constant and not distorted, and the frequency results may be more accurate. For each IMF the frequency is calculated using FFT, and the results are illustrated in 7.7.

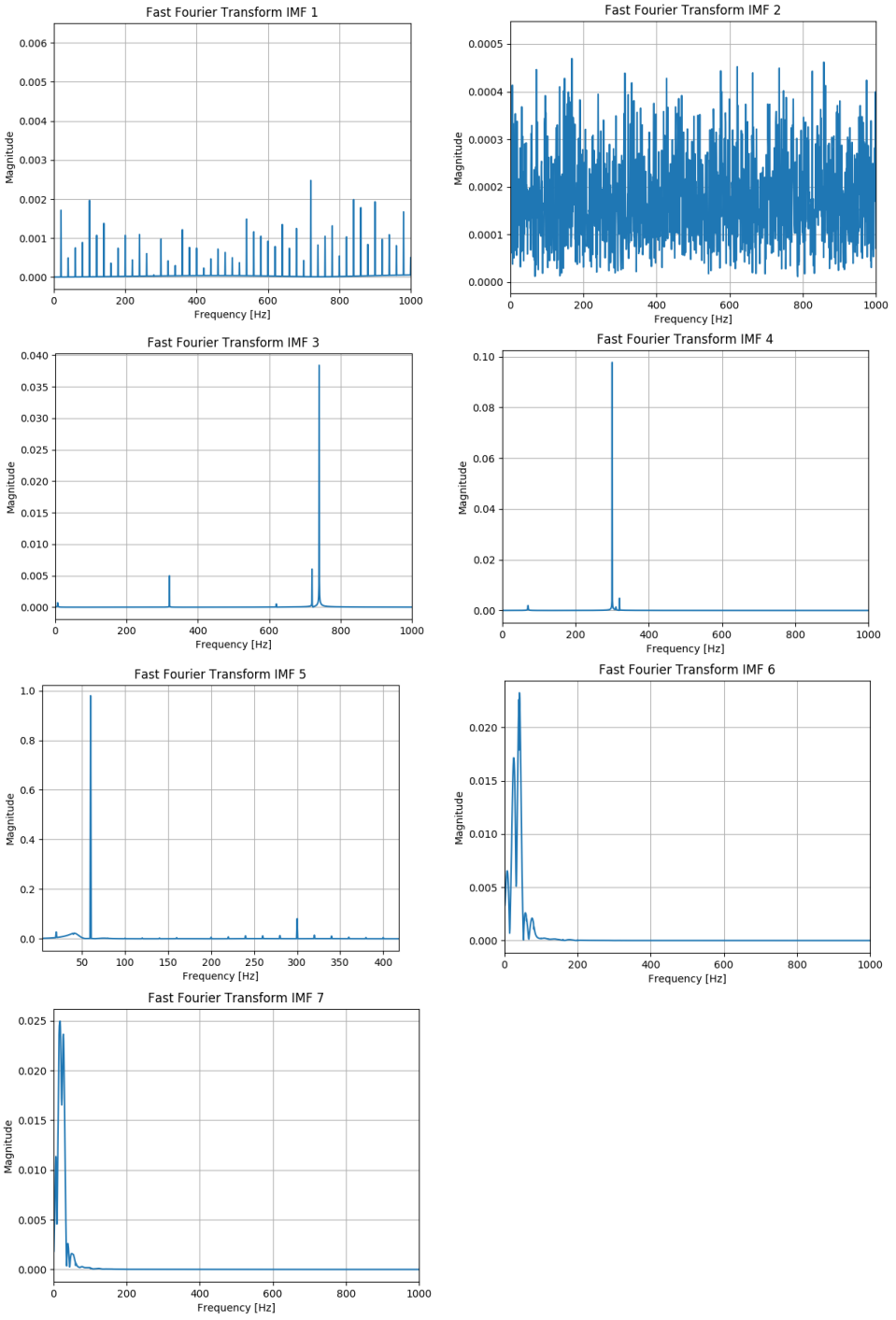

Figure 7.7: Frequency results of IMF 1 - IMF 7 using FFT.

Based on the frequency results illustrated in Figure 7.7, it is concluded that IMF 1 and IMF 2 represents the noise present in the duplicated current signal. The next IMFs, IMF 3, IMF 4 and IMF 5, have amplitudes that correspond to the amplitudes obtained in 7.3, and are considered as the main components that carry information about the frequency components present in the signal. The FFT result of IMF 3 reveals a dominating frequency component at 740 Hz with an amplitude just below 0.04, but it also contain a frequency component at approximately 300 Hz and one at approximately 700 Hz, both with a small amplitude around 0.005. The same goes for the other two functions, IMF 4 and IMF 5, where other small frequency components are present in the FFT results. This reveals that there is mode mixing present, but the main frequency component for each IMF is still detected using the FFT.

7.2 Part 2 - Analysis using the standard EMD (MATLAB code)

In this section, the standard EMD will be applied to both the original current measurement in Figure 7.1 and the duplicated signal in Figure 7.2 using a MATLAB implementation of the EMD. After the decomposition is complete, the frequencies will be calculated using both instantaneous frequency and FFT.

7.2.1 Original current signal

The original current measurement is analyzed using a MATLAB implementation of the standard EMD. The analysis was performed using 8 siftings as the stopping criteria, as this gave the most accurate results. The result of the decomposition using the standard EMD is illustrated in Figure 7.8.

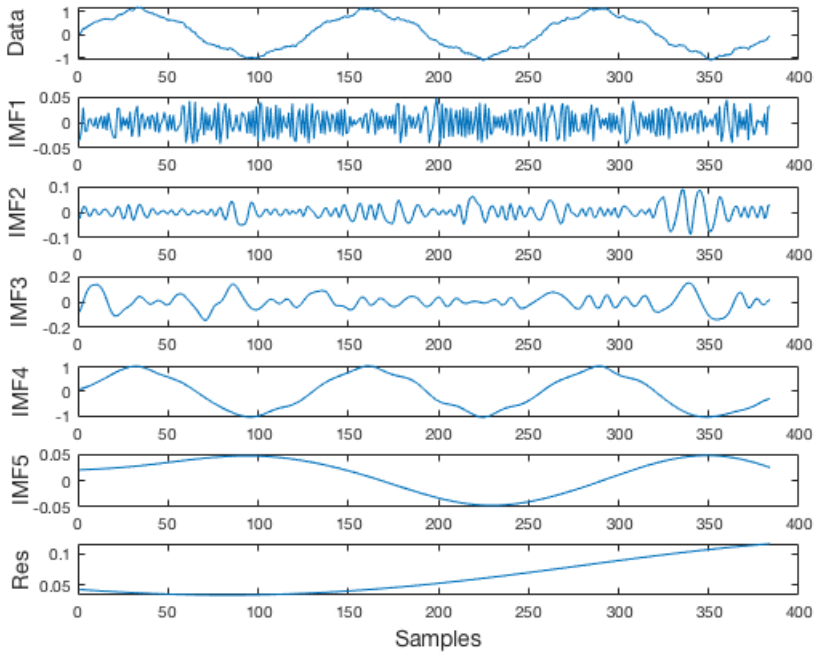

Figure 7.8: EMD of the original current signal using 8 siftings as the stopping criteria.

The decomposition, illustrated in Figure 7.8, reveals 5 IMFs, which is one less IMF than the decomposition using the Python implementation of the standard EMD provides. The reason for this can be explained by the number of siftings, which are different for the two cases, and that they are two different implementation of the standard EMD. The IMFs in Figure 7.8 are not as influenced by end effect like the IMFs in Figure 7.3, which is an improvement. On the other hand, the IMFs in Figure 7.3 are more distorted than the IMFs in Figure 7.8.

As for the results obtained by the standard EMD in Python, the instantaneous frequency of each IMF and the FFT of the original current measurement are calculated. The results are illustrated in Figure 7.9.

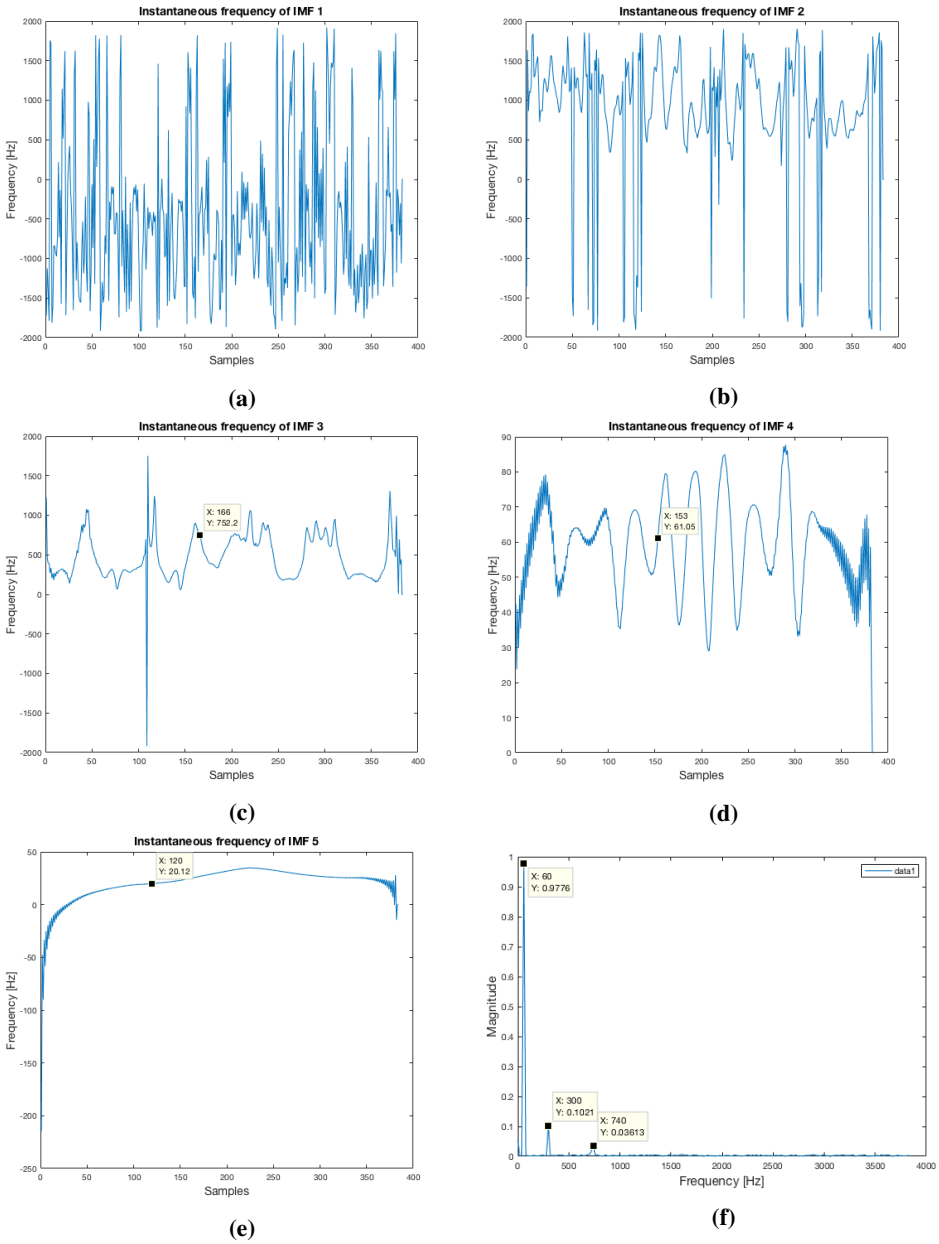

Figure 7.9: a) Instantaneous frequency of IMF 1, b) instantaneous frequency of IMF 2, c) instantaneous frequency of IMF 3, d) instantaneous frequency of IMF 4, e) instantaneous frequency of IMF 5, f) FFT of the original current measurement.

Based on the frequency results illustrated in Figure 7.9, the first IMF that resembles any of the frequency components is IMF 3. As for the results obtained with the standard EMD in Python, this IMF reveals a oscillating frequency between 500 Hz and 1000 Hz. Purely based on this frequency result, it is not possible to confirm that this is one of the frequency components of the signal. On the other hand, since the standard EMD in Python revealed a similar frequency result for this IMF, and the FFT result of the signal in Figure 7.9 f shows a frequency component of 740 Hz, it can be concluded that this IMF carries information about this frequency component. IMF 4 on the other hand reveals a completely different results than the results obtained with the standard EMD in Python. In Figure 7.9 d, the frequency oscillates between 30 Hz and 90 Hz, and it is not possible to extract any of the other two frequency components. Even though the average of the frequency is approximately 60 Hz, it is clear that it is influenced by another frequency component. Thus, it can be concluded that this decomposition suffers from mode mixing, and the 300 Hz component and the 60 Hz component are not detected.

7.2.2 Duplicated current signal

As for the analysis performed in Python, the duplicated signal illustrated in Figure 7.2 is also analyzed using the standard EMD in MATLAB. The analysis is performed using the stopping criteria of 8 siftings. The decomposition using the standard EMD in MATLAB is illustrated in Figure 7.10.

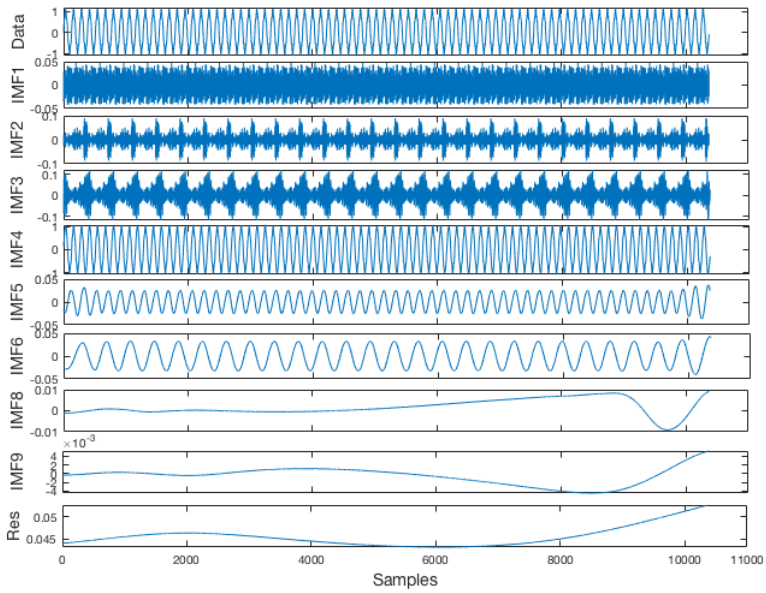

Figure 7.10: EMD of the duplicated current signal using 8 siftings as the stopping criteria.

The decomposition in Figure 7.10 reveals 9 IMFs, which is two more than the decompo-

sition of the same signal using the standard EMD in Python. As for the results obtained for the original signal using the standard EMD in MATLAB, the end effects are still improved compared to the results obtained by the standard EMD in Python. As for the other analyses using the standard EMD, the frequencies of the IMFs are calculated. For a proper comparison, the frequencies are calculated in the same way as for duplicated signal using the standard EMD in Python, by using FFT. The frequency results are illustrated in Figure 7.11.

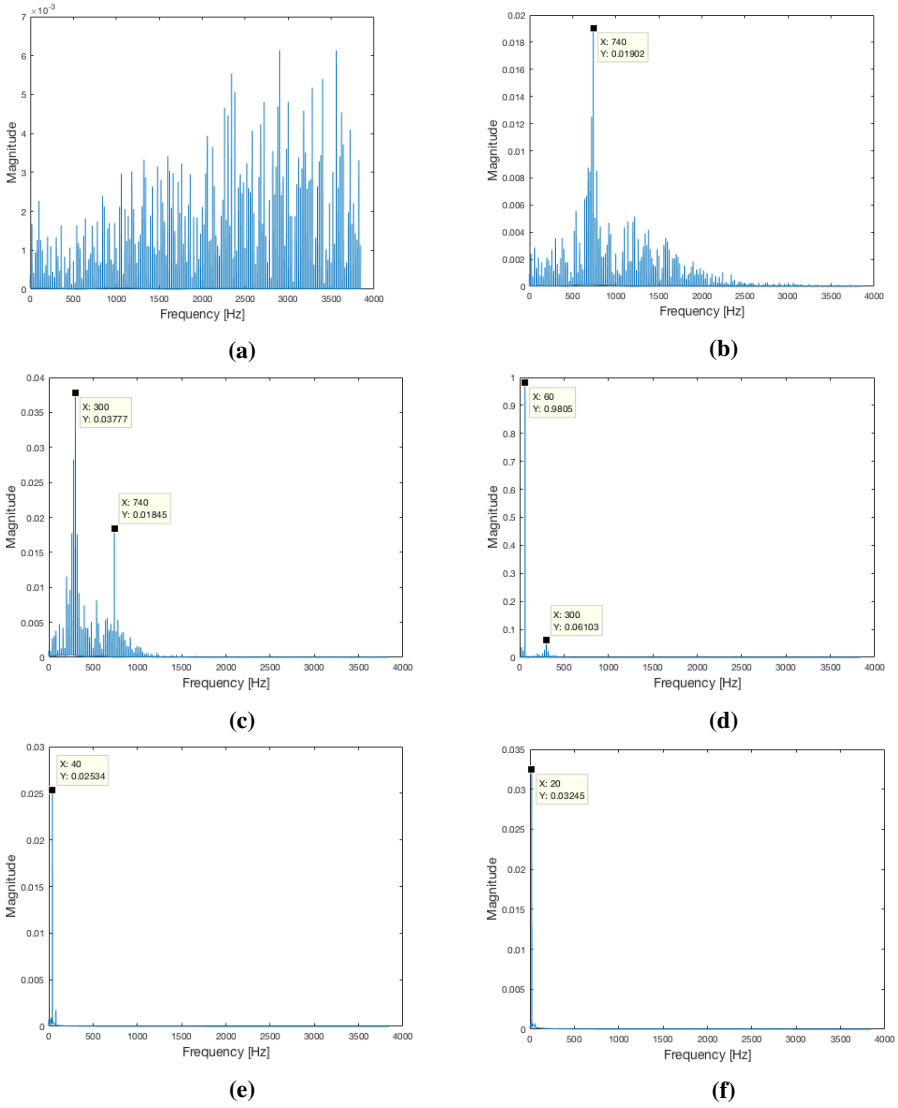

Figure 7.11: a) FFT of IMF 1, b) FFT of IMF 2, c) FFT of IMF 3, c) FFT of IMF 4, d) FFT of IMF 5 and e) FFT of IMF 6.

In Figure 7.11, the second IMF, IMF 2, reveals a dominating frequency of 740 Hz with an amplitude just below 0.02, and multiple of components with smaller amplitudes both with higher and lower frequency. Because of the small amplitude and the presence of other components it is clear that there is mode mixing present. Since the amplitude of the 740 Hz is too low, it can be assumed that the component is also present in IMF 3. In IMF 3, the dominating frequency component is the 300 Hz component, but the 740 Hz component is also present. The 300 Hz component has a too low amplitude, and it is clear that the frequency component must be present in other IMFs. In IMF 4 a frequency component at 60 Hz with an amplitude just below 1 is detected. In addition to this a frequency component at 300 Hz is detected as well. Based on this it is clear to say that the frequency component of 300 Hz is both present in IMF 4 and in IMF 3, and that mode mixing is present in more than one case. Mode mixing is also present in the results obtained with Python, but in Python, the results are a bit more accurate for the IMFs.

Based on these results obtained by the standard EMD, both in Python and MATLAB, it can be seen that the Python implementation of the standard EMD provides the most accurate decomposition both for the original signal and the duplicated signal.

7.3 Part 3 - Analysis using the online EMD

In this part the online EMD is used to analyze the duplicated signal illustrated in Figure 7.2. As mentioned earlier in the results, the online EMD and the standard EMD use the same implementation of the standard EMD. The online EMD applies the standard EMD in a window, then the window is shifted. Before the duplicated signal is analyzed, the online EMD is applied to a synthetic signal in order to demonstrate the working principle of the method.

7.3.1 Synthetic signal 1

In this section, a synthetic signal is analyzed in order to verify the decomposition and to illustrated the working principle of the online EMD. The synthetic signal consists of three sinusoids with frequencies of 25 Hz, 80 Hz and 800 Hz, all with amplitude 1, and a linear trend. The online EMD is applied with 4 siftings as the stopping criteria and with 10 extrema per window ($l = 10$).

Figures 7.12, 7.13 and 7.14 illustrates the decomposition using online EMD after 500, 1500 and 4500 samples, respectively. After 500 samples, Figure 7.12, the IMF with the highest frequency is extracted, while the other components are still in the residual. At the moment that there are $l = 10$ extrema in the residual, the online EMD starts to extract the second IMF and after that, it extracts IMF 3 (Figures 7.13 and 7.14). The red parts in the plots are the parts of the IMFs that are not completed yet due to the stitching procedure. These parts indicate the delay of each IMF (time delay, Δt), which is determined by the frequency of the IMF.

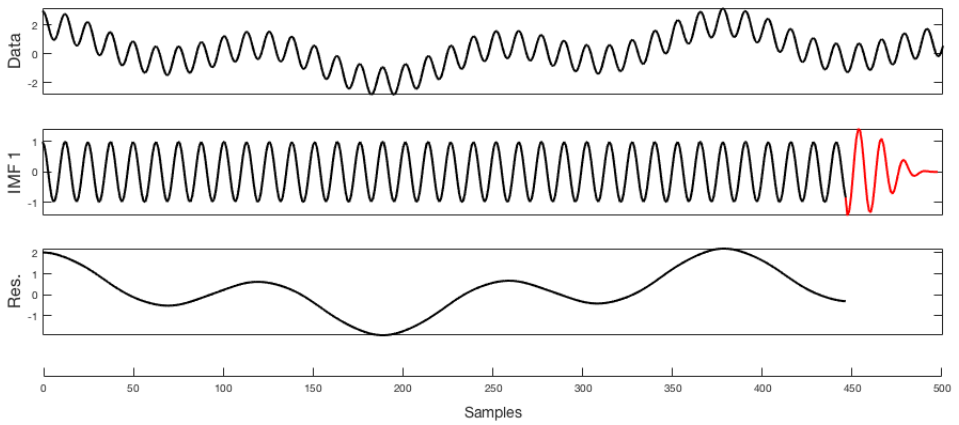

Figure 7.12: Decomposition of a synthetic signal using online EMD after analyzing 500 samples. The window size is 10, i.e., l=10 and 4 siftings is used.

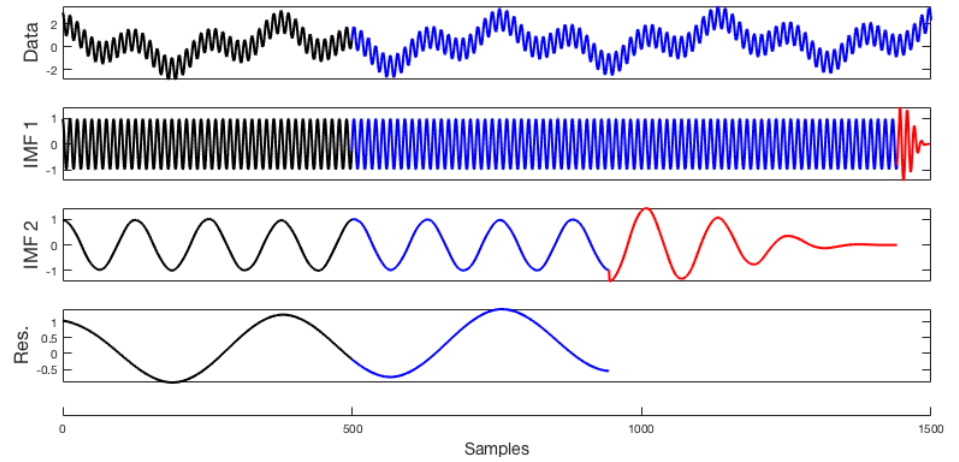

Figure 7.13: Decomposition of a synthetic signal using online EMD after analyzing 1500 samples. The red parts are the parts of the IMFs that are still incomplete. The window size is 10 , i.e., l=10 and 4 siftings is used.

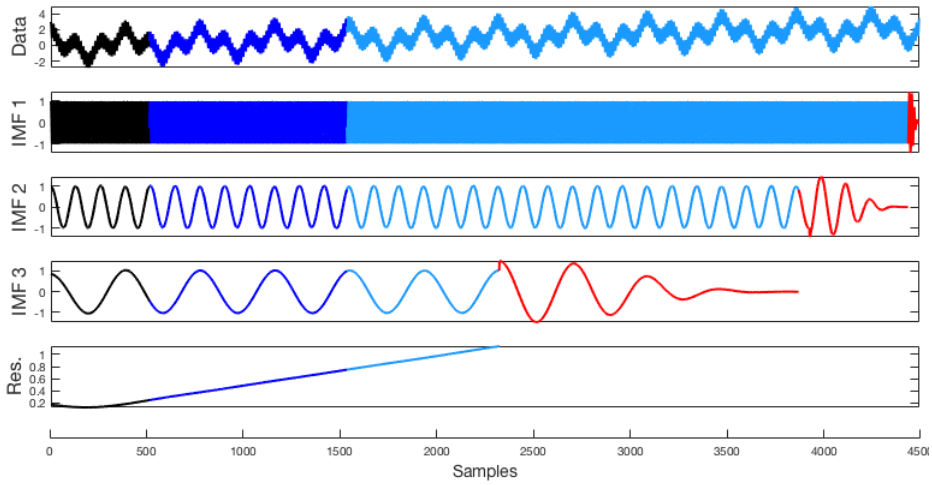

Figure 7.14: Decomposition of a synthetic signal using online EMD after analyzing 4500 samples. The red parts are the parts of the IMFs that are still incomplete. The window size is 10 , i.e., l=10, and a 4 siftings is used.

The decomposition using the online EMD on this synthetic signal reveals 3 IMFs. The decomposition after 4500 samples, illustrated in Figure 7.14, shows a promising decomposition where the IMFs look even and not distorted. After the decomposition was completed, the instantaneous frequency for each of the IMFs was calculated. The calculation of the instantaneous frequencies was performed using the algorithm presented in section 6.2.1 and the results are illustrated in Figures 7.15, 7.16 and 7.17.

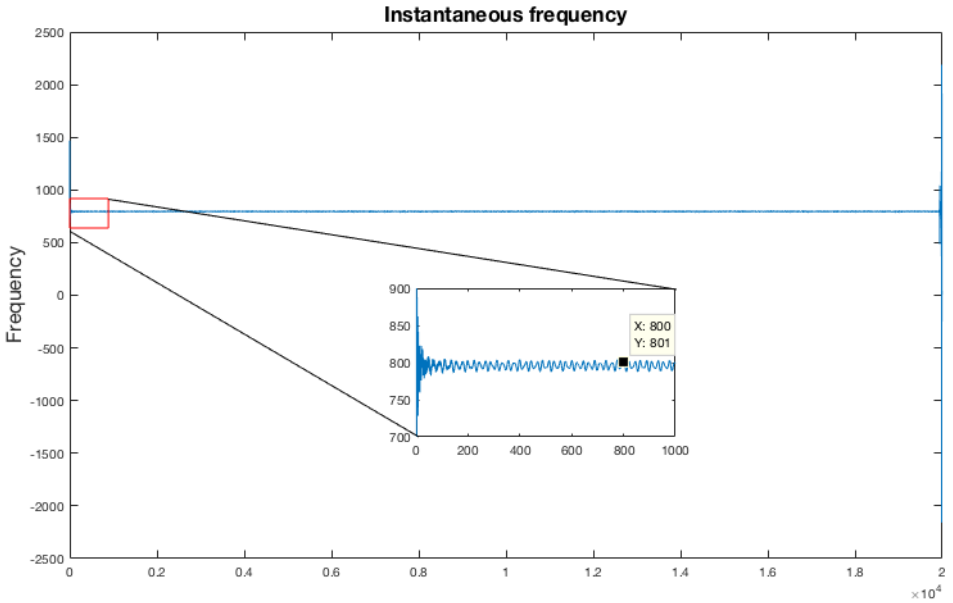

Figure 7.15: Instantaneous frequency of IMF 1. The samples are shown on the x-axis, and the Frequency, in Hertz, on the y-axis.

Figure 7.15 shows the instantaneous frequency of IMF 1. The result reveals that a frequency of approximately 800 Hz is discovered, which corresponds to the highest frequency component of the synthetic signal. The frequency is constant for the whole sampling period, only with few deviations.

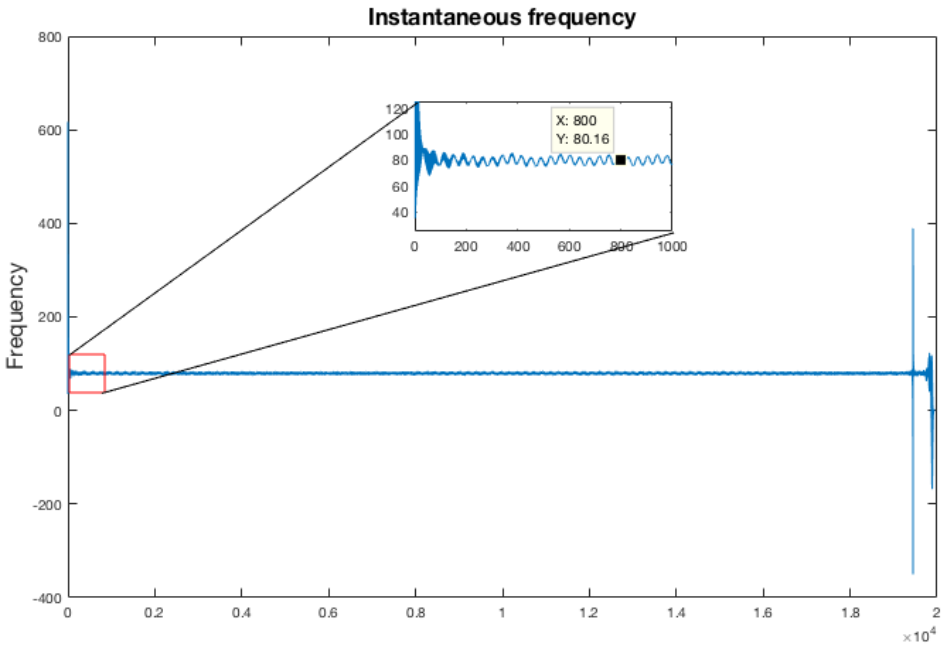

Figure 7.16: Instantaneous frequency of IMF 2. The samples are shown on the x-axis, and the Frequency, in Hertz, on the y-axis.

Figure 7.16 shows the instantaneous frequency of IMF 2. The result shows that a frequency of approximately 80 Hz is discovered, which corresponds to one component of the synthetic signal. The frequency is constant in large parts of the result, but deviates a bit at the end. This deviation does not influence a large part of the result, and it can still be concluded, that the frequency component of 80 Hz is properly detected.

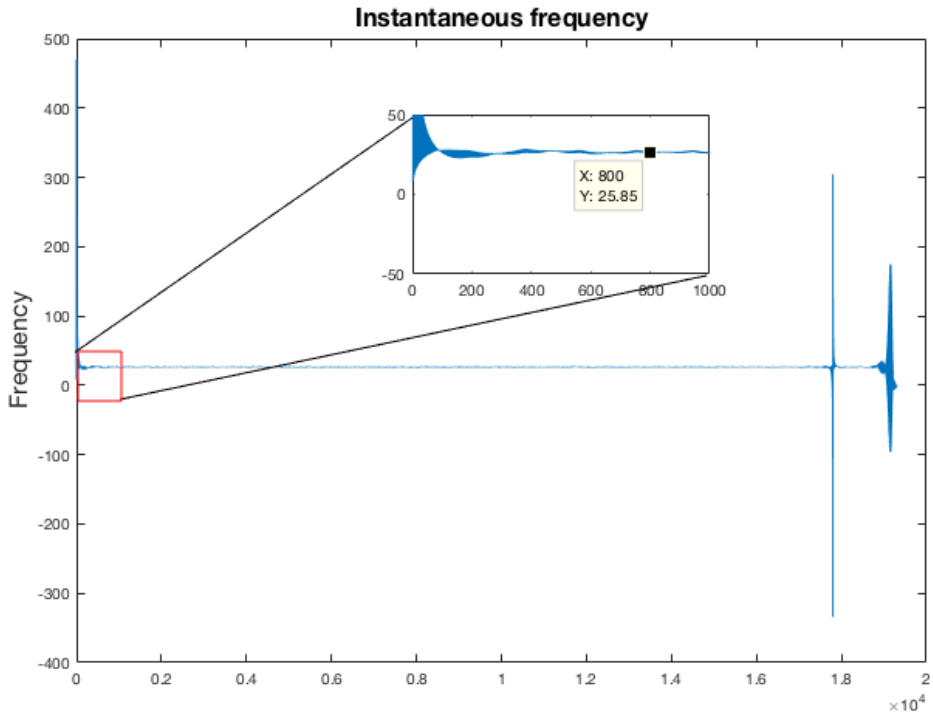

Figure 7.17: Instantaneous frequency of IMF 3. The samples are shown on the x-axis, and the Frequency, in Hertz, on the y-axis.

Figure 7.17 shows the instantaneous frequency of IMF 3. The result shows that a frequency of approximately 25 Hz is discovered, which corresponds to the lowest frequency component of the synthetic signal. The frequency obtained here is even more constant than the frequency for IMF 1 and IMF 2. Even though it is more constant for the most part, it shows a larger devuation at the end than the other two IMFs. The deviation however, does not influence the correct detection of the 25 Hz component.

The decomposition using online EMD and the instantaneous frequency calculation shows accurate results for the synthetic signal, and the working principle of the online EMD is well illustrated by this example.

7.3.2 Analysis of duplicated current signal

Since the original current measurement illustrated in 7.1 is only 0.05 seconds long and only contains 6 extrema, the duplicated current signal illustrated in Figure 7.2 will be analyzed using the online EMD. The online EMD was applied with 10 extrema per window ($l = 10$) and with 8 siftings. The results of the online EMD revealed 18 IMFs. Since the purpose of the analysis is to examine harmonic components, only the IMFs with such relevance are shown in Figure 7.18. The complete results of the online EMD can be seen in the Appendix.

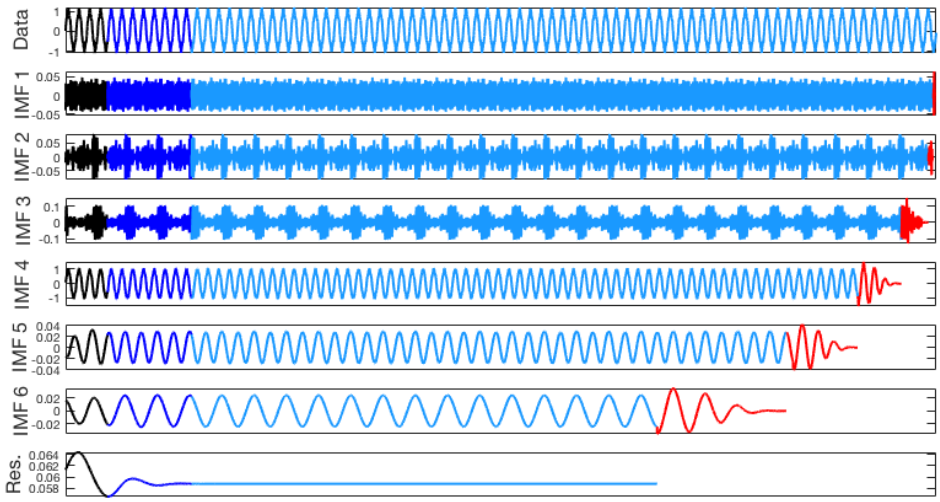

Figure 7.18: Online EMD of the duplicated signal with 8 siftings, window size $l = 10$ and only showing 6 IMFs.

In Figure 7.18, only the IMFs with relevance is presented. Based on prior analysis of this signal, and the original signal, the decomposition raises some concerns. The IMFs have a too low amplitude to be considered as one of the frequency components of the signal, and there might be a mode mixing issue. The instantaneous frequency of the 6 IMFs is calculated and the results are illustrated in Figure 7.19.

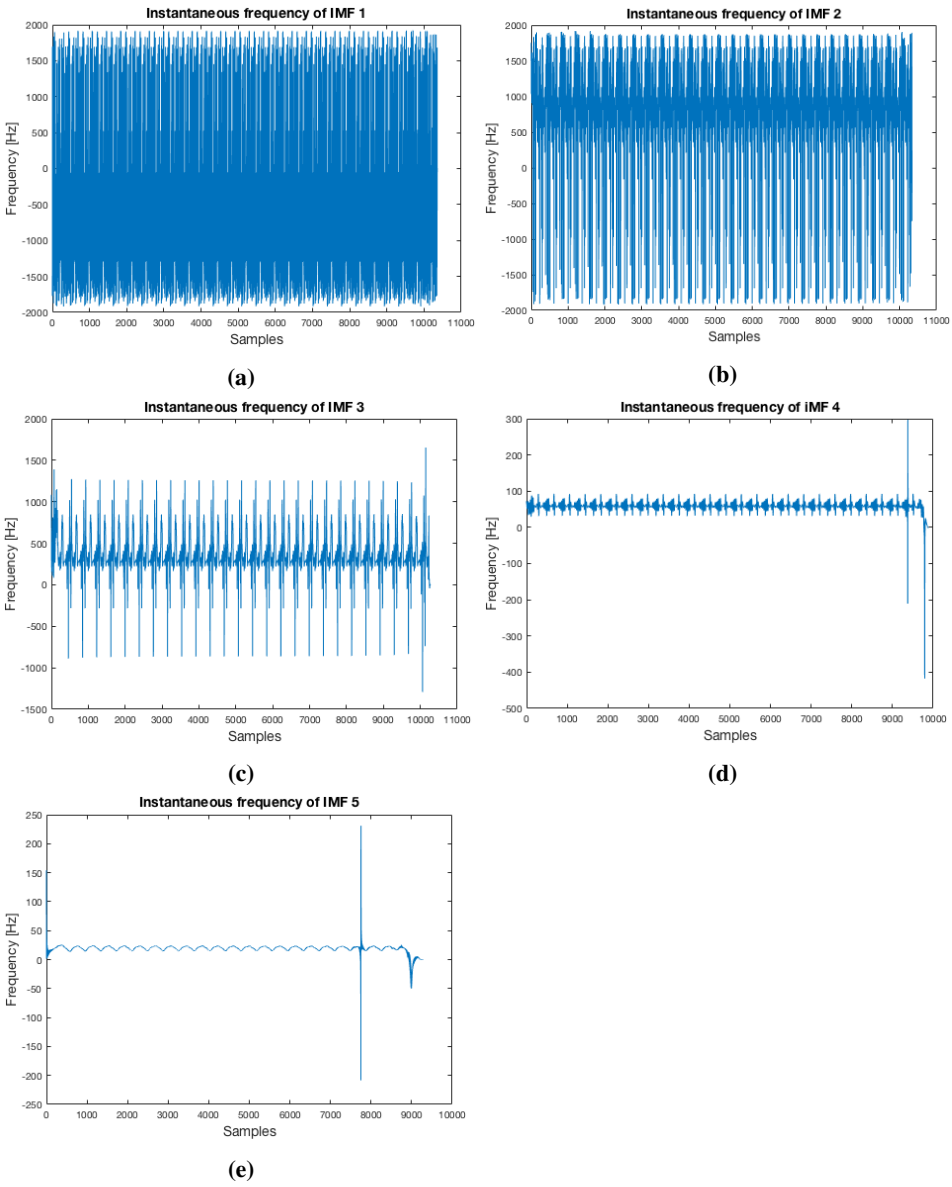

Figure 7.19: a) Instantaneous frequency of IMF 1, b) instantaneous frequency of IMF 2, c) instantaneous frequency of IMF 3, c) instantaneous frequency of IMF 4, d) instantaneous frequency of IMF 5 and e) instantaneous frequency of IMF 6.

As for the results obtained with the standard EMD in MATLAB, the online EMD suffers from mode mixing for this particular signal as the IMFs reveal a oscillating frequency. The first IMF in Figure 7.19, IMF 1, is considered as noise. The frequency result of IMF 2, IMF 3 and IMF 4 reveals fluctuating frequencies and it is clear that there is mode mixing present. From the frequency result of these three IMFs it is not possible to extract any of the frequency components. From the results of IMF 4 the average frequency might be approximately 60 Hz, but it is influenced by another frequency component in some parts. IMF 5 and IMF 6 reveals more constant frequency results, but the frequencies are two low to be considered as one of the frequency components of the signal. It is clear that the decomposition is not accurate for the duplicated signal both using the standard EMD and the online EMD in MATLAB.

7.3.3 Synthetic signal 2

Because the online EMD of the duplicated current signal revealed mode mixing, online EMD is applied to a signal with the same properties as the constructed signal in Figure 7.5 but with the same length as the duplicated signal, 1.35 seconds, in order to examine the decomposition when there is no noise in the signal. The duplicated signal and the reconstruction are illustrated in Figure 7.20 and 7.21. The decomposition of the online EMD, using 8 siftings, is illustrated in Figure 7.22.

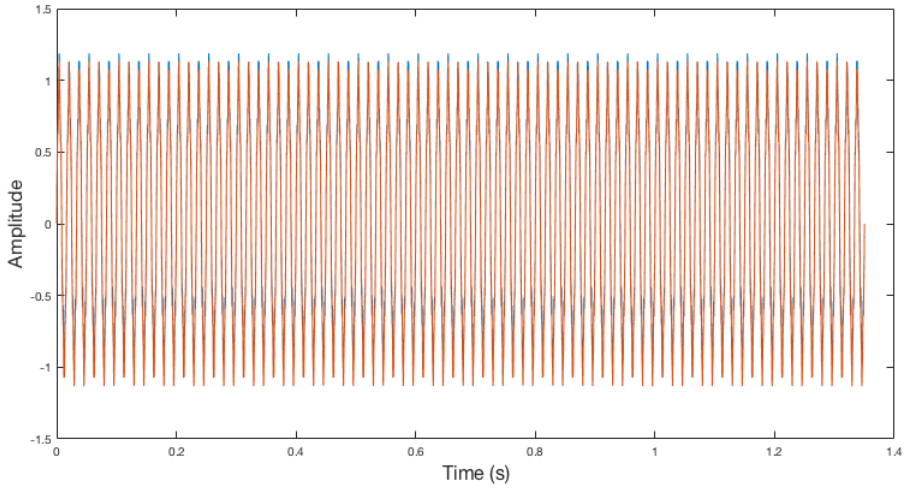

Figure 7.20: Plot showing the synthetic signal $\sin(2\pi 60t) + 0.1\sin(2\pi 300t) + 0.04\sin(2\pi 740t)$ in orange and the duplicated signal in blue for the entire time span.

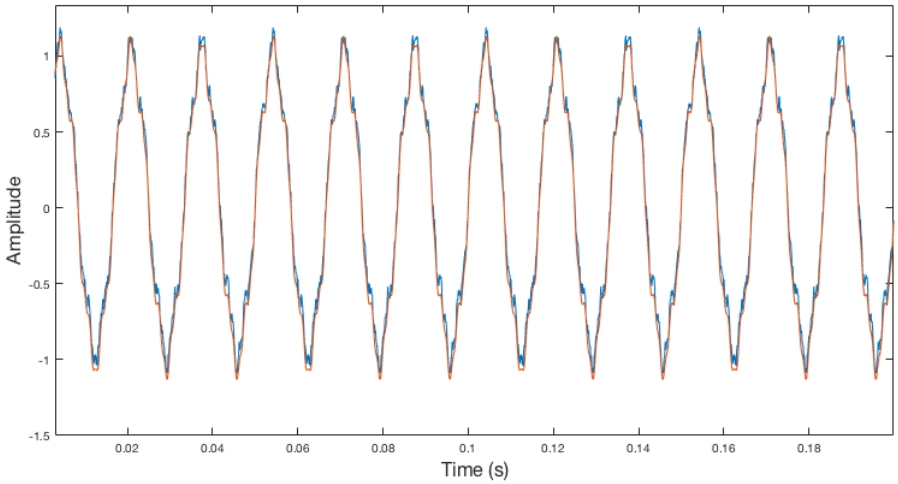

Figure 7.21: Plot showing the synthetic signal $\sin(2\pi 60t) + 0.1\sin(2\pi 300t) + 0.04\sin(2\pi 740t)$ in orange and the duplicated signal in blue for 0.2 seconds.

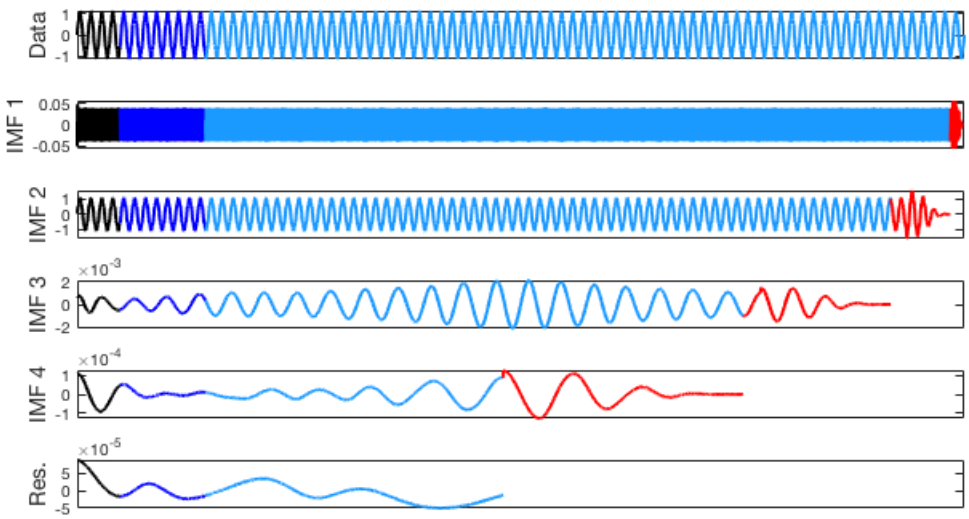

Figure 7.22: Online EMD of the synthetic signal $\sin(2\pi 60t) + 0.1\sin(2\pi 300t) + 0.04\sin(2\pi 740t)$ with the window size $(l) = 10$ and with 8 siftings.

The decomposition of the synthetic signal using online EMD in Figure 7.22 reveals 4 IMFs. IMF 1 and IMF 2 looks constant, while IMF 3 and IMF 4 reveals a change in the oscillation in the middle part. This might indicate that there is something happening in the middle of the IMFs, and that IMF 2 and IMF 3 might be influenced with some deviations

as well. The instantaneous frequency of each of the IMFs is calculated and the results are illustrated in Figure 7.23.

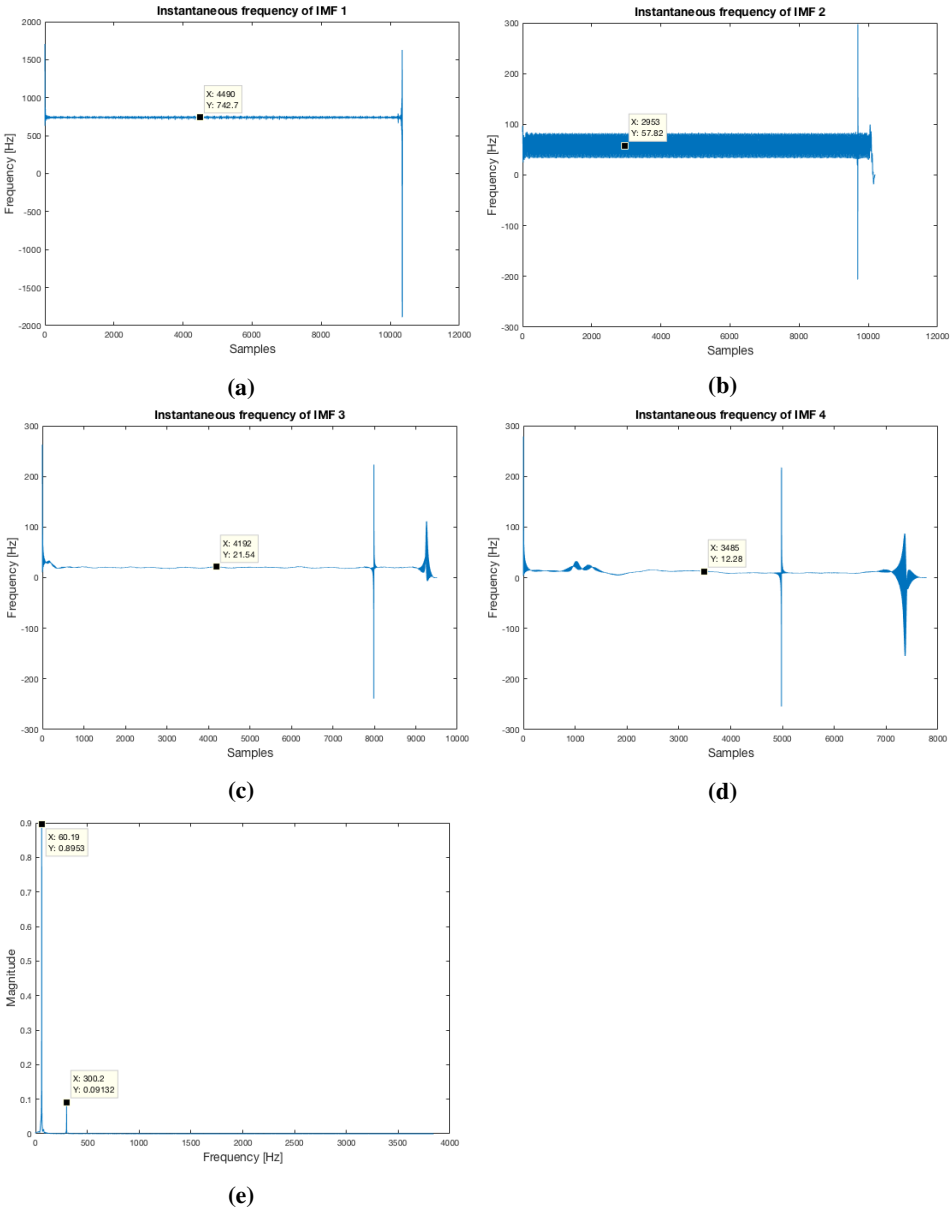

Figure 7.23: a) Instantaneous frequency of IMF 1, b) instantaneous frequency of IMF 2, c) instantaneous frequency of IMF 3, d) instantaneous frequency of IMF 4 and e) FFT of IMF 2.

Compared to the decomposition achieved from the duplicated current signal using the online EMD method, the decomposition of the synthetic signal is improved. In Figure 7.23, the 740 Hz component is detected properly in IMF 1, but the 300 Hz is still not detected in IMF 2. IMF 2 shows a fluctuating frequency around 60 Hz. In figure 7.23 e, the FFT is applied to IMF 2, and the results reveal a frequency component of 60 Hz and one at 300 Hz. This indicates that there is still mode mixing between the 60 Hz and the 300 Hz frequency component.

7.3.4 Synthetic signal 3

The mode mixing effect from the EMD became clear after the original signal was duplicated to make it longer for the online EMD analysis. In order to examine the time delay of the IMF components for a case when mode mixing does not occur, another synthetic signal was constructed. Through trial and error it was found that the amplitudes presented in Table 7.1 gave results without mode mixing. The synthetic signal is then composed as $\sin(2\pi 60t) + 0.2\sin(2\pi 300t) + 0.08\sin(2\pi 740t)$. The decomposition of the online EMD is illustrated in Figure 7.24.

Table 7.1: Table showing the frequency and amplitudes of the frequency components of the synthetic signal.

Component	Frequency [Hz]	Amplitude
1	740	0.08
2	300	0.2
3	60	1

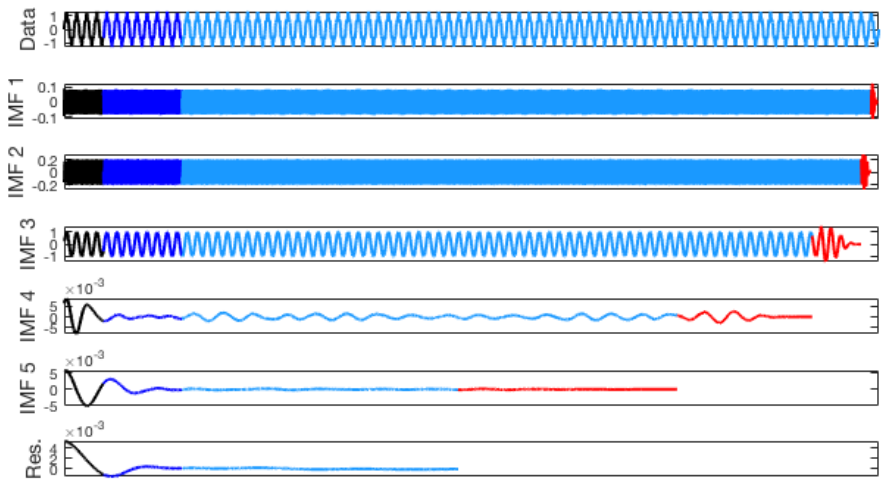

Figure 7.24: Online EMD of the synthetic signal $\sin(2\pi 60t) + 0.2\sin(2\pi 300t) + 0.08\sin(2\pi 740t)$.

The decomposition in Figure 7.24 reveals 5 IMFs. The first three IMFs is expected to be the once carrying information about the frequency components of the signal as the last two IMFs are of small amplitude. For each of the IMFs, the instantaneous frequency is calculated. The frequency results are illustrated in Figure 7.25.

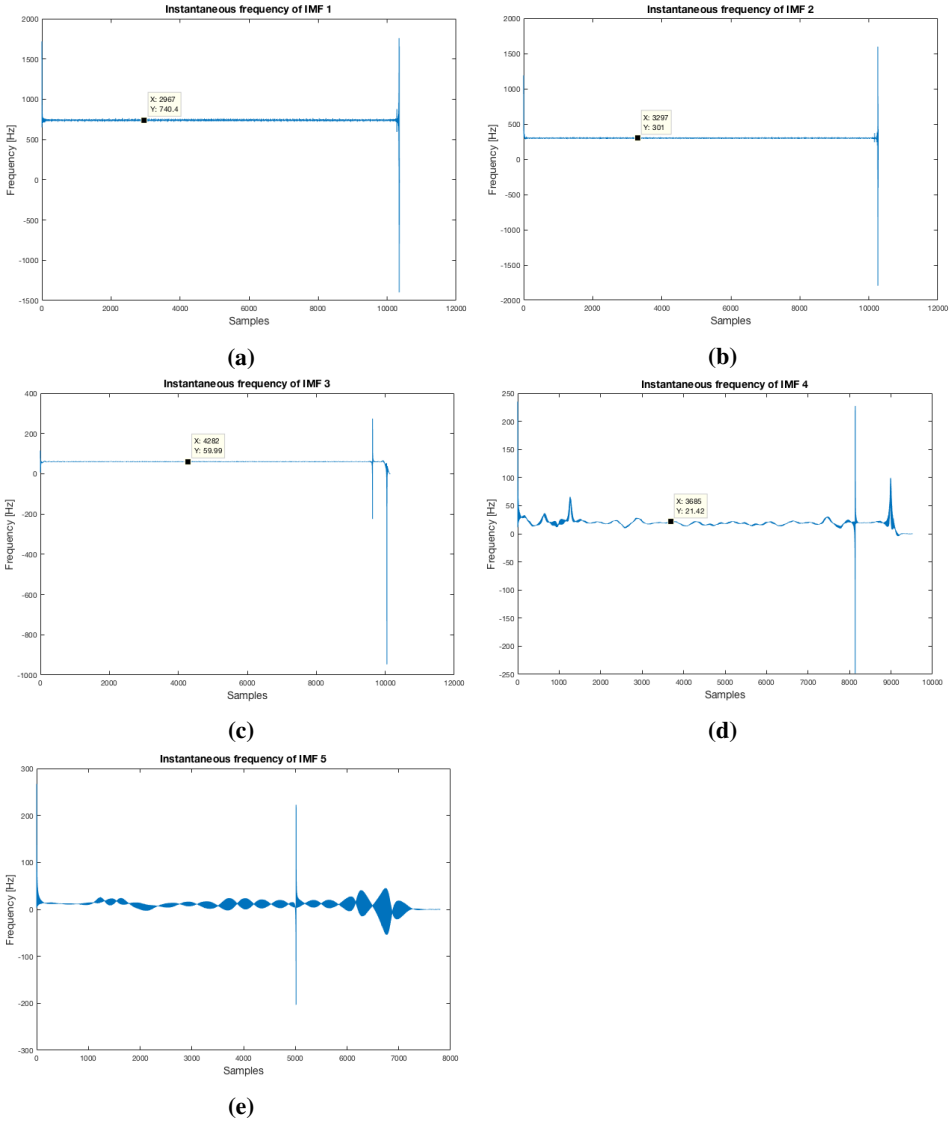

Figure 7.25: a) Instantaneous frequency of IMF 1, b) instantaneous frequency of IMF 2, c) instantaneous frequency of IMF 3, d) instantaneous frequency of IMF 4 and e) and instantaneous frequency of IMF 5.

The frequency results in Figure 7.25, reveal accurate frequency results. IMF 1 reveals a frequency of 740 Hz, IMF 2 reveals a frequency of 300 Hz and IMF 3 reveals a frequency of 60 Hz, which corresponds to the frequency components of the synthetic signal. Hence, by increasing the amplitudes of the two harmonic components, a proper decomposition without mode mixing is achieved.

7.3.5 Time delay of IMFs

The red part of the IMFs in Figure 7.24 illustrates the part of the signal that is not completed yet bacause of the stitching procedure in the online EMD. This indicates that for each IMF, there is a time delay, Δt, which increases from one IMF to another. Since the EMD extracts the fastest oscillation first, the time delay for components with lower frequency will be longer than the time delay for the components with higher frequency. The time delays are presented in Table 7.2. In the case of harmonic detection, it is only necessary to consider the time delays for the components representing the harmonic components. For this signal, this includes IMF 1, IMF 2 and IMF 3.

Table 7.2: Time delays for each IMF obtained with the online EMD and $l = 10$.

Component	Time delay (s)
IMF 1	0.0112
IMF 2	0.0267
IMF 3	0.0961
IMF 4	0.2906
IMF 5	0.6971

The time delay of each IMF represents the time required by the online decomposition process to obtain an IMF for real-time applications. For example, IMF 2 is obtained about 0.03 seconds after the measured signal is available. However, in the standard EMD decomposition process, the full signal has to analyzed, which is not suitable for real-time applications.

Chapter 8

Conclusion and further work

The standard EMD and the online EMD have been studied and applied to signals containing harmonics. For the original current measurement, mode mixing did not occur for the Python code for standard EMD, but it did occur for the MATLAB code for standard EMD. For the duplicated version of the current measurement, mode mixing occurred for both the Python code of standard EMD and the MATLAB codes for standard EMD and online EMD. The mode mixing was more severe for the MATLAB codes for both standard EMD and online EMD, than it was for the Python code of the standard EMD. The online EMD and standard EMD in MATLAB uses the same algorithm for EMD, and since both of them experienced mode mixing, it is concluded that the mode mixing is a problem for the EMD algorithm, not the online implementation of the standard EMD. It can be concluded that the Python code for EMD handles mode mixing more properly than the MATLAB codes for online EMD and standard EMD, but as seen from the results, the MATLAB codes for online EMD and standard EMD handles the end effects in a more proper way than the Python code for standard EMD.

The EMD implementation in Python and the implementation in MATLAB are suppose to perform the same task, but as seen in the results, they provide different results. Different methods used in either the interpolated curves between extrema or to minimize end effects might be the cause of the different results obtained for Python and MATLAB results. The online EMD is an open source code, which can be downloaded and used by anybody. What the analysis in this thesis has shown is that it is important to fully understand what the method does, and that there might be other implementations of the same method that are more suited for the particular signal. With empirical methods, it is important to fully understand the premise and the working principle of the method in order to choose the right parameters.

It is not ideal to duplicate a current measurement since it is no longer an actual measurement, and the mode mixing got worse in this case. In order to investigate the mode mixing issue, a synthetic signal was constructed based on the frequency results obtained by the standard EMD in Python. The synthetic signal was analyzed using the online EMD, and it revealed that there was still mode mixing present. Since the frequencies are far apart (60 Hz, 300 Hz and 740 Hz), it was concluded that it was the amplitudes of these frequency components that caused the mode mixing. Through trial and error, it was found that when the amplitudes of the harmonic components were doubled, mode mixing did not occur, and a proper decomposition was obtained.

The method is called online EMD, but as revealed in the results, the method impose a time delay to the IMFs, making it not completely online. The time delay can be reduced by changing the number of siftings and the window size, but as the method is now, it is only suitable for window sizes of more than 10 extrema.

Even though the results revealed mode mixing for the specific current measurement, there are, as mentioned, solutions to this problem. The online EMD provides more opportunities, like analyzing data streams, which would be beneficial for control purposes in for example active power filters. Because of this, the method should be pursued in the future.

Concluding remarks

- Online EMD is an extension of the EMD that enables analysis of data streams, which is beneficial for control purposes in for example active power filters.
- There are different ways to implement the EMD method in both MATLAB and Python, and in this thesis a comparison of two chosen implementations is performed. The standard EMD and the online EMD implementations in MATLAB are more prone to mode mixing than the standard EMD implementation in Python for this specific current measurement.
- The end effects are more severe in the standard EMD implementation in Python than for the standard EMD and Online EMD implementations in MATLAB.
- When the amplitudes of the current harmonics in the current measurements are doubled, mode mixing does not occur.
- Even though the method is called online EMD, the method imposes a time delay to each of the IMFs, which makes the method not completely online.

Further work

For further analysis using the online EMD the author has some suggestions for further work:

- The online EMD is a newer extension that should be applied for other current measurements containing harmonics, preferably for measurements that does not have to be duplicated, in order to further grasp the accuracy of the decomposition.
- Based on the mode mixing problem, methods for suppressing such phenomena should be implemented in the code. Since the mode mixing was not as severe in the Python code, another implementation of the EMD might improve the results obtained with the MATLAB codes for both standard EMD and online EMD. One possibility is to investigate if a different interpolation improves the results.
- Since the online EMD is able to analyze data streams, the method should be pursued for control purposes in for example active power filters.

Bibliography

[1] W Mack Grady and Surya Santoso. “Understanding power system harmonics”. In: *IEEE Power Engineering Review* 21.11 (2001), pp. 8–11.

[2] JC Das. *Power system harmonics and passive filter designs*. John Wiley & Sons, 2015.

[3] Norden E Huang et al. “The empirical mode decomposition and the Hilbert spectrum for nonlinear and non-stationary time series analysis”. In: *Proceedings of the Royal Society of London. Series A: Mathematical, Physical and Engineering Sciences* 454.1971 (1998), pp. 903–995.

[4] Jean-Claude Nunes and Eric Deléchelle. “Empirical mode decomposition: Applications on signal and image processing”. In: *Advances in Adaptive Data Analysis* 1 (2009).

[5] Romain Fontugne, Pierre Borgnat, and Patrick Flandrin. “Online empirical mode decomposition”. In: *2017 IEEE International Conference on Acoustics, Speech and Signal Processing (ICASSP)*. IEEE. 2017, pp. 4306–4310.

[6] Jos Arrillaga and Neville R Watson. *Power system harmonics*. John Wiley & Sons, 2004.

[7] Hirofumi Akagi. “New trends in active filters for improving power quality”. In: *Proceedings of International Conference on Power Electronics, Drives and Energy Systems for Industrial Growth*. Vol. 1. IEEE. 1996, pp. 417–425.

[8] Stuti Shukla, S Mishra, and Bhim Singh. “Online EMD with Fourier Transform for active shunt filter operation under non sinusoidal supply conditions”. In: *2012 IEEE International Conference on Power Electronics, Drives and Energy Systems (PEDES)*. IEEE. 2012, pp. 1–5.

[9] GK Singh. “Power system harmonics research: a survey”. In: *European Transactions on Electrical Power* 19.2 (2009), pp. 151–172.

[10] Edward L Owen. “A history of harmonics in power systems”. In: *IEEE Industry Applications Magazine* 4.1 (1998), pp. 6–12.

[11] Martine Johanne N Baksvaer. “Harmonic propagation in microgrid power converters and harmonic identification techniques”. In: (Dec. 2018).

[12] Francisco C. De La Rosa. *Harmonics and Power Systems*. 1. Taylor & Francis Group, 2006.
[13] Robert G Ellis and P Eng. "Power system harmonics–a reference guide to causes, effects and corrective measures". In: *An Allen-Brandley Series of Issues and Answers-Rockwell Automation* (2001), p. 3.
[14] David Chapman. "Harmonics: Causes and effects". In: *Power Quality Application Guide* 3 (2001).
[15] Johan HR Enslin and Peter JM Heskes. "Harmonic interaction between a large number of distributed power inverters and the distribution network". In: *IEEE transactions on power electronics* 19.6 (2004), pp. 1586–1593.
[16] John HR Enslin et al. "Harmonic interaction between large numbers of photovoltaic inverters and the distribution network". In: *Power Tech Conference Proceedings, 2003 IEEE Bologna*. Vol. 3. IEEE. 2003, 6–pp.
[17] Jegatheeswaran Thambirajah, Emilio Barocio, and Nina F Thornhill. "Comparative review of methods for stability monitoring in electrical power systems and vibrating structures". In: *IET generation, transmission & distribution* 4.10 (2010), pp. 1086–1103.
[18] Toshihiko Tanaka and Hirofumi Akagi. "A new method of harmonic power detection based on the instantaneous active power in three-phase circuits". In: *IEEE transactions on power delivery* 10.4 (1995), pp. 1737–1742.
[19] N Pecharanin, H Mitsui, and M Sone. "Harmonic detection by using neural network". In: *Proceedings of ICNN'95-International Conference on Neural Networks*. Vol. 2. IEEE. 1995, pp. 923–926.
[20] Hong-bin Pan et al. "An improved adaptive harmonic detection method based on least squares algorithm". In: *PROCEEDINGS-CHINESE SOCIETY OF ELECTRICAL ENGINEERING* 28.13 (2008), p. 144.
[21] Lucian Asiminoaei, Frede Blaabjerg, and Steffan Hansen. "Evaluation of harmonic detection methods for active power filter applications". In: *Twentieth Annual IEEE Applied Power Electronics Conference and Exposition, 2005. APEC 2005.* Vol. 1. IEEE. 2005, pp. 635–641.
[22] Peter J Brockwell, Richard A Davis, and Stephen E Fienberg. *Time Series: Theory and Methods: Theory and Methods*. Springer Science & Business Media, 1991.
[23] Angela Zeiler et al. "Empirical mode decomposition-an introduction". In: *The 2010 International Joint Conference on Neural Networks (IJCNN)*. IEEE. 2010, pp. 1–8.
[24] Ya-juan Xue et al. "Does mode mixing matter in EMD-based highlight volume methods for hydrocarbon detection? Experimental evidence". In: *Journal of Applied Geophysics* 132 (2016), pp. 193–210.
[25] Maximiliano López et al. "The Mode Mixing Problem and its Influence in the Neural Activity Reconstruction". In: *IAENG International Journal of Computer Science* 46 (Apr. 2019).
[26] Yunchao Gao et al. "Analysis and solution to the mode mixing phenomenon in EMD". In: *2008 Congress on Image and Signal Processing*. Vol. 5. IEEE. 2008, pp. 223–227.
[27] Donghoh Kim and Hee-Seok Oh. "EMD: a package for empirical mode decomposition and Hilbert spectrum". In: *The R Journal* 1 (2009), pp. 40–46.

[28] MC Peel, GGS Pegram, and TA McMahon. “Empirical mode decomposition: improvement and application”. In: *Proc. Int. Congress Modelling Simulation*. Vol. 1. 2007, pp. 2996–3002.

[29] Jen-Chun Lee et al. “Recognizing human iris by modified empirical mode decomposition”. In: *Pacific-Rim Symposium on Image and Video Technology*. Springer. 2007, pp. 298–310.

[30] Sylvain Meignen and Valérie Perrier. “A new formulation for empirical mode decomposition based on constrained optimization”. In: *IEEE Signal Processing Letters* 14.12 (2007), pp. 932–935.

[31] Gabriel Rilling, Patrick Flandrin, Paulo Goncalves, et al. “On empirical mode decomposition and its algorithms”. In: *IEEE-EURASIP workshop on nonlinear signal and image processing*. Vol. 3. NSIP-03, Grado (I). 2003, pp. 8–11.

[32] Francis HS Chiew et al. “Identification of oscillations in historical global streamflow data using empirical mode decomposition”. In: *Proc. 7th IAHS Scientific Assembly* (2005), pp. 53–62.

[33] Zhaohua Wu and Norden E Huang. “Ensemble empirical mode decomposition: a noise-assisted data analysis method”. In: *Advances in adaptive data analysis* 1 (2009), pp. 1–41.

[34] Rupert Faltermeier et al. “Weighted sliding empirical mode decomposition”. In: *Advances in Adaptive Data Analysis* 3.04 (2011), pp. 509–526.

[35] Michael Feldman. *Hilbert transform applications in mechanical vibration*. John Wiley & Sons, 2011.

[36] D De Yong, S Bhowmik, and Fernando Magnago. “An effective power quality classifier using wavelet transform and support vector machines”. In: *Expert Systems with Applications* 42.15-16 (2015), pp. 6075–6081.

Appendix

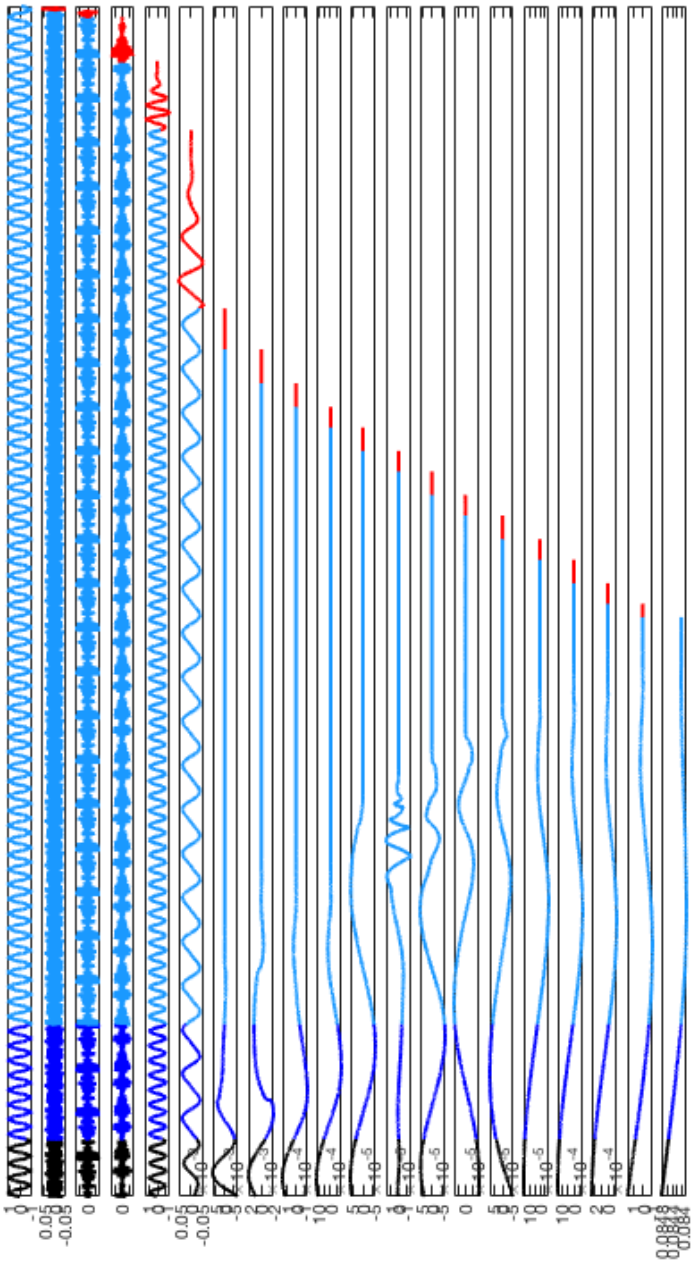

Figure 8.1: Online EMD of duplicated current signal with infinite IMFs and 8 siftings. The first is the plot of the data, the next 18 plots are the IMFs, and the last one is the residue.

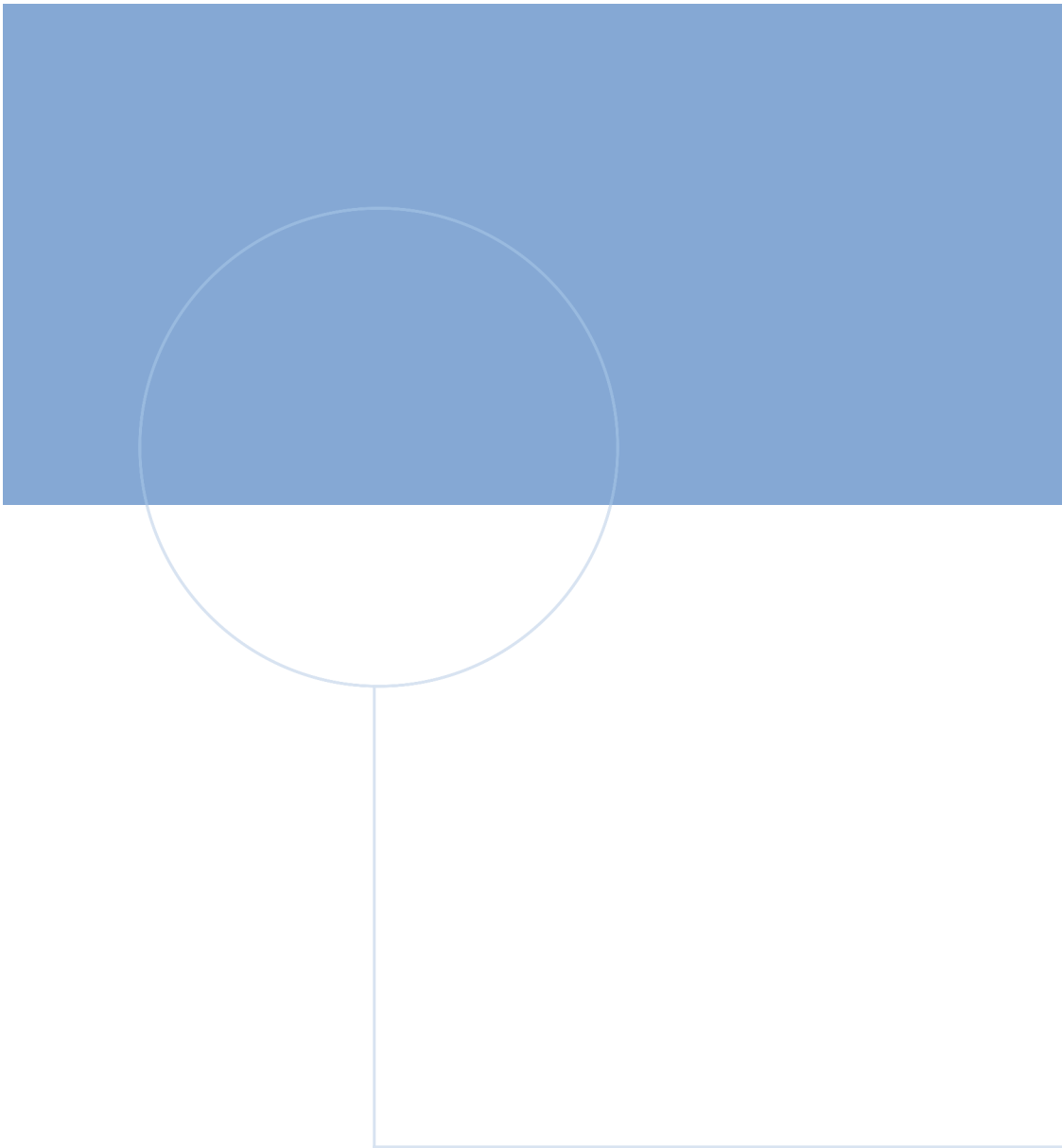

NTNU
Norwegian University of
Science and Technology